The differential metabolic signature of breast cancer cellular response to olaparib treatment

Domenica Berardi[1], Yasmin Hunter[1], Lisa van den Driest[1], Gillian Farrell[1], Nicholas J W Rattray[1*], and Zahra Rattray[1*]

1. Strathclyde Institute of Pharmacy and Biomedical Sciences, University of Strathclyde, Glasgow, G4 0RE.

Corresponding authors: zahra.rattray@strath.ac.uk and nicholas.rattray@strath.ac.uk

ABSTRACT

Metabolic reprogramming and genomic instability are key hallmarks of cancer, the combined analysis of which has gained recent popularity. Given the emerging evidence indicating the role of oncometabolites in DNA damage repair and its routine use in breast cancer treatment, it is timely to fingerprint the impact of olaparib treatment in cellular metabolism. Here, we report the biomolecular response of breast cancer cell lines with DNA damage repair defects to olaparib exposure.

Following evaluation of olaparib sensitivity in breast cancer cell lines, we immunoprobed DNA double strand break foci and evaluated changes in cellular metabolism at various olaparib treatment doses using untargeted mass spectrometry-based metabolomics analysis. Following identification of altered features, we performed pathway enrichment analysis to measure key metabolic changes occurring in response to olaparib treatment.

We show a cell-line dependent response to olaparib exposure, and an increased susceptibility to DNA damage foci accumulation in triple-negative breast cancer cell lines. Metabolic changes in response to olaparib treatment were cell-line and dose- dependent, where we predominantly observed metabolic reprogramming of glutamine-derived amino acids and lipids metabolism.

Our work demonstrates the effectiveness of combining molecular biology and metabolomics studies for the comprehensive characterisation of cell lines with different genetic profiles. Follow-on studies are needed to map the baseline metabolism of breast cancer cells and their unique response to drug treatment. Fused with genomic and transcriptomics data, such readout can be used to identify key oncometabolites and inform the rationale for the design of novel drugs or chemotherapy combinations.

KEYWORDS: Breast cancer, triple-negative, oncometabolites, DNA damage, precision medicine, metabolic reprogramming

INTRODUCTION

In a bid to develop new therapies against various cancer types, genomic instability, its underpinning mechanisms and contribution to tumorigenesis have been extensively investigated over the past few decades. Genomic instability, a well-known contributor to cancer, presents a therapeutic vulnerability that can be targeted in the development of novel chemotherapy agents (1).

To maintain their genomic integrity, cells are equipped with a range of DNA damage repair (DDR) pathways and responses to counteract DNA lesions formed in response to endogenous and exogenous insults (2). Hereditary mutations in these pathways have been correlated with increased cancer susceptibility, such that defects in homologous recombination contribute to approximately 10% of all breast cancers. These defects in DDR machinery result in the loss of function for genes implicated in DNA repair (i.e. breast cancer susceptibility gene 1/2-BRCA1/BRCA2) or dysregulation of cell cycle phases (3-5). While these genetic alterations increase the susceptibility to oncogenesis- they serve as therapeutic vulnerabilities- such that

in the presence of a defective DNA repair pathway the inhibition of an alternate DDR mechanism will lead to cell death. This concept is referred to as synthetic lethality, which has formed the rationale for existing DDR inhibitors (6,7). One such class of drugs, poly(ADP-ribose) polymerase (PARP) inhibitors, targets vulnerabilities in the homologous recombination DDR pathway (8).

PARP inhibitors as a class of DDR inhibitors block the activity of PARP enzymes involved in DNA damage repair; therefore, leading to accumulation of DNA double-strand breaks that gives rise to genomic instability and subsequent apoptosis (9). Several PARP inhibitors are currently approved as monotherapies for the treatment of locally advanced or metastatic breast cancer for patients with breast cancer harboring germline BRCA1/2 mutations or HER2-negative receptor status (8). In 2022, olaparib was approved by the FDA as an adjuvant treatment for patients with human epidermal growth factor receptor 2 (HER2)-negative and germline BRCA-mutated breast cancers following readout from the OlympiA trial (10).

While PARP inhibitors present a therapeutic opportunity for targeting DDR defects in breast and ovarian cancers, emerging evidence has shown a role for oncometabolites- small molecule intermediates of cellular metabolism- in determining the response to these chemotherapies. The biology of oncometabolites and their role in modulating DDR has been increasingly studied over the past few years, guiding new combination therapies and novel biological targets for drug discovery (1).

Metabolic reprogramming- a key feature of all cancers (11)- gives rise to chemoresistance in both treatment-naïve and treatment-resistant breast cancers (12). As with genomic instability, drivers of metabolic reprogramming can be broadly classified as intrinsic and extrinsic in origin (13). Intrinsic stimuli such as oncogenes and tumour suppressor genes, modulate cellular metabolism in breast cancer with several regulators including BRCA1/2, MYC, phosphatidylinositol-4,5-bisphosphate 3-kinase (PI3K) and p53 as examples. The functional interplay between these regulators of cellular metabolism, mediates DNA damage repair pathways and subsequent response to DDR chemotherapies. Recent evidence has shown that the upregulation of glucose utilization and glutamine metabolism are required to sustain increased tumour bioenergetic and biosynthetic demand, which vary according to the cellular genetic makeup (14). Intermediates from glucose and glutamine metabolism have been identified as key oncometabolites regulating the response to chemotherapy drugs, presenting novel biomarkers and potential actionable targets for novel drug discovery (13).

DDR mechanisms induce cellular metabolic changes through interference with purine and pyrimidine biosynthetic pathways, amino acid metabolism, protein biosynthesis and energy metabolism, impacting several metabolic routes (15). Mediators of DDR pathways, including PARP regulate several pathways exemplified by the pentose-phosphatase pathway, the TCA cycle and glycolysis. In breast cancer, PARP inhibition reduces glucose consumption and alters amino acid and nucleotide metabolism depending on the different cellular subtypes (16). Moreover, BRCA-1 deficient breast tumors appear to rely on glucose consumption through enhanced glycolysis (17). Differences in the metabolic signature between cell lines harboring different DNA repair mutations and measuring their response to PARP inhibitors can inform the rationale for selecting PARP inhibitors in certain breast cancer types and explore potential additional vulnerabilities as druggable targets (18).

DNA repair and regulation of metabolism are critical for maintaining homeostasis in normal human cells. However, the extensive dysregulation and aberrant function of both these pathways promotes tumorigenesis. Until recent, DNA repair and metabolic pathways have routinely been researched as distinct fields within their own right, but growing emerging research evidence an intrinsic inter-dependency between these pathways. Here, we report the differential cellular response of breast cancer cell lines with DDR defects to olaparib exposure through combined analysis of DNA damage and metabolomics profiling. Combined

evaluation of the DNA damage response and metabolic reprogramming offers new opportunities in the development of novel chemotherapies against cancer.

MATERIALS

Cell lines and chemicals

All cell lines used in this study were purchased from the vendor and maintained in accordance with manufacturer instructions. All cell culture reagents were obtained from Gibco (Thermo Fisher Scientific). MCF7 (RRID:CVCL_0031, Sigma, EACC collection) and MDA-MB-231 cells (RRID:CVCL_0062, ATCC) were purchased and maintained in Dulbecco's Modified Eagle Medium (DMEM, high glucose) supplemented with 10% *v/v* FBS (high glucose, Invitrogen), 1% *v/v* non-essential amino acids (NEAA) and 1% *v/v* penicillin-streptomycin (Invitrogen). Corresponding cell line origins, hormone receptor status and mutational profiles are included in **Table 1**. HCC1937 cells obtained from ATCC (RRID:CVCL_0290) were maintained in RPMI supplemented with 10% *v/v* FBS and 1% v/v penicillin-streptomycin. All cell lines were maintained at 37 °C in a pre-humidified atmosphere containing 5% *v/v* CO_2 and used within ten passages for the purposes of this work (passage 2-10).

Olaparib (SantaCruz Biotechnology Inc.) was prepared as a 100 mM stock solution in DMSO, aliquoted and stored at -20 °C until use. γH2AX, p53BP1 primary antibodies (Cell Signalling Technologies) were used for foci immunostaining alongside the Alexa Fluor® 488-conjugated secondary antibody (Fisher Scientific).

Table 1 *Cell lines used in this study and their corresponding clinicopathologic profiles (ER: estrogen receptor, PR: progesterone receptor, and HER2: Human epidermal growth factor 2 receptor)*

Cell Line	Histology	Subtype	Immunoprofile	Genetic alterations
MCF-7	Metastatic Adenocarcinoma	Luminal A	ER+, PR+, HER2-	PIK3CA, CDKN2A, GATA3, PIK3CA, TP53
MDA-MB-231	Metastatic Adenocarcinoma	Basal	ER-, PR-, HER2-	BRAF, CDKN2A, KRAS, NF2, TP53
HCC1937	Primary Ductalcarcinoma	Basal-like	ER-, PR-, HER2-	BRCA1, TP53

METHODS

Cell Viability Assays

MCF-7, MDA-MB-231 and HCC1937 cells undergoing exponential growth were seeded at a density of 4,000 cells/well in 96 well plates and incubated overnight to facilitate cell attachment. On the following day, cells were exposed to either blank growth medium (control) or growth medium containing different concentrations of olaparib (treatment medium) ranging from 0.01-500 μM for seven days at 37 °C and 5% *v/v* CO_2. Treatment media were replaced every three days with treatment medium. Following a seven day treatment, cell viability was measured using CellTiter 96® Aqueous Non-Radioactive Cell Proliferation Assay (Promega) (3-(4,5-dimethylthiazol-2-yl)-5-(3-carboxymethoxyphenyl)-2-(4-sulfophenyl)-2H-tetrazolium (MTS) reagent. The resultant absorbance at 490 nm was measured using a model GM3500 Glomax® Explorer Multimode Microplate Reader (Promega).

Growth curves represent percentage cell growth following treatment with different concentrations of olaparib and are plotted as a semi-log dose-response curve. The half maximal inhibitory concentration (IC_{50}) was determined using a linear regression model. Statistical analysis was performed using GraphPad Prism (RRID:SCR_002798, v.9.0.1). Three independent biological replicates (five wells per treatment concentration) were performed for each cell line.

Immunostaining for γH2AX and p53BP1

Foci immunodetection for γH2AX and p53BP1 was performed in both control (growth medium) and for cells treated with olaparib (IC_{10}, IC_{25} and IC_{50} doses) for seven days. Briefly, cell monolayers were fixed in chilled 4% *w/v* formaldehyde containing 2% *w/v* sucrose in PBS, followed by fixation in ice-cold methanol (100% v/v). Subsequently, cells were permeabilized in 0.25% *v/v* Triton X-100 in PBS, blocked with 5% *v/v* goat serum/5% *w/v* BSA, immunoprobed with either a primary rabbit anti- γH2AX antibody (RRID:AB_420030) (1:1000) or primary rabbit anti-P53BP1 (1:200) antibody (RRID:AB_11211252, CST #2675 for p53BP1) overnight at 4 °C. Cell monolayers were treated with goat, anti-rabbit Alexa Fluor® 488 conjugated secondary antibody and counterstained with DAPI. Image acquisition was carried out using an Invitrogen EVOS Auto Imaging System (AMAFD1000-Thermo Fisher Scientific) with a minimum of 100 cells imaged per treatment condition. Resultant foci images were analysed in Cell Profiler (v.4.2.1.) using a modified version of the speckle counting pipeline.

Sample preparation and metabolite extraction

MCF-7, MDA-MB-231 and HCC1937 cells were seeded at a density of 2 x 10^6 cells per well in 6-well plates, and exposed to growth medium containing olaparib at IC_{10}, IC_{25} and IC_{50} doses, as determined from the MTS assay (n=5 per treatment concentration). Following exposure to olaparib, the growth medium was aspirated from each well, centrifuged to remove cell debris, and stored at -80 °C. Next, treated cells were washed with pre-chilled PBS, with the metabolites quenched and extracted in a final volume of 1.5 mL pre-chilled (-80°C) mixed solvent (Methanol:Acetonitrile:Water=50:30:20). Resultant cell pellets were collected, and submerged in liquid nitrogen, vortexed and sonicated for 3 minutes in an ice-water bath. This procedure was performed in triplicate. Resultant extracts were centrifuged at 13,000x g for 10 minutes at 4 °C and the pellets were retained for protein quantification using the Bradford assay. The resultant supernatant was collected, and dried with a Speed vac centrifuge (Savant-SPD121P). Dried metabolite pellets were reconstituted in Acetonitrile:Water (50:50) at volumes normalized to the relative protein content. Quality control (QC) samples were prepared by pooling samples across all control and treatment groups. Solvent blank and QC samples were inserted in analytical batch after every five samples to assess the stability of detecting system.

Liquid Chromatography Tandem Mass Spectrometry (LC-MS/MS)

Metabolite separation was performed on a binary Thermo Vanquish ultra high performance liquid chromatography system where 5µl of reconstituted cellular extract was injected on to a Thermo Accucore HILIC column (100mm x 2.1 mm, particle size 2.6 µm). The temperature of the column oven was maintained at 35 °C while the autosampler temperature was set at 5 °C. For chromatographic separation a consistent flow rate of 500 µl/min was used where the mobile phase in positive heated electrospray ionisation mode (HESI+) was composed of buffer A (10 mM ammonium formate in 95% acetonitrile, 5% Water with 0.1% formic acid) and buffer B (10 mM ammonium formate in 50% acetonitrile, 50% Water in 0.1% formic acid). Likewise, in negative ionisation mode (HESI-) buffer A (10 mM ammonium acetate in 95% acetonitrile, 5% water with 0.1% acetic acid) and buffer B (10 mM ammonium acetate in 50% acetonitrile, 50% water with 0.1% acetic acid). The elution gradient used for the chromatographic separation of metabolites is included in supplementary information.

A high-resolution Exploris 240-Orbitrap mass spectrometer (ThermoFisher Scientific) performed full scan and fragmentation analyses. Global operating parameters were set as follows: spray voltages of 3900 V in HESI+ mode, and 2700 V in HESI- mode. The temperature of transfer tube was set as 320 °C with a vaporiser temperature of 300 °C. Sheath, aux gas and sheath gas flow rates were set at 40, 10 and 1 Arb, respectively. Data dependent acquistions (DDA) were performed using the following parameters: full scan range was 70 – 1050 m/z with a MS1 resolution of 60,000. Subsequent MS/MS scans were processed with a resolution of 15,000. High-purity nitrogen was used as nebulising gas and as the collision gas for higher energy collisional dissociation. Further details are included in supplementary information.

Mass Spectrometry Data Processing

Raw data files obtained from Thermo Scientific Xcalibur™ software 4.2 were imported into the Compound Discoverer™ 3.2 software (CD) where the “Untargeted Metabolomics with Statistics Detect Unknowns with ID Using Online Databases and mzLogic” feature was selected (supplementary information). The workflow analysis performs retention time alignment, unknown compound detection, predicts elemental compositions for all compounds, and hides chemical background (using Blank samples). For the detection of compounds, mass and retention time (RT) tolerance were set to 3 ppm and 0.3 min, respectively. The library search was conducted against the mzCloud, Human Metabolome Database (HMDB) and Chemical Entities of Biological Interest (ChEBI) database. A compound table was generated with a list of putative metabolites (known and unknown). Among them, we selected all the

known compounds fully matching at least two of the annotation sources. The selected metabolites were then used to perform pathway and statistical analysis.

Pathway Analysis with MetaboAnalyst

Prior to analysis of the metabolic pathways with MetaboAnalyst 5.0 (RRID:SCR_015539, https://www.metaboanalyst.ca/), a HMDB identification code was assigned to each selected metabolite. A joint pathway analysis was performed by integrating the genes relative to each cell line (Table 1) with the list of ID compounds and their associated Log2 Fold change values. The integration method combined both genes and metabolites into a single query, then used to perform the enrichment analysis. This latter was based on a hypergeometric test. Finally, important nodes (compounds) were scored based on their betweenness centrality, and pathway analysis results were generated.

Statistical Analysis

All data are presented as mean ± standard deviation (n≥5). For metabolomics analysis, Principal Component Analysis (PCA) was performed to test analytical reproducibility of QC injections, reduce the dimensionality of our data and determine the metabolic profiles of the different sample groups. Differential analysis was also used to compare differences between control and treatment groups, then plotted in a Volcano plot (log-fold change vs. -log10 p-value). Peak areas were $\log_{10}$ transformed and p values were calculated for the sample group by analysis of variance (ANOVA) test. A p value<0.05 and fold-change of 1.5 was deemed to be statistically significant.

RESULTS

Olaparib sensitivity analysis

To determine the olaparib dose range for subsequent foci and metabolomics experiments, we measured the sensitivity of MCF7, MDA-MB-231 and HCC1937 cell lines to olaparib exposure over a seven day treatment duration. The rationale behind exploring sensitivity to olaparib in these cell lines, was to perform a comparison between two triple-negative (MDA-MB-231 and HCC1937) and a non triple-negative (MCF-7) cell line.

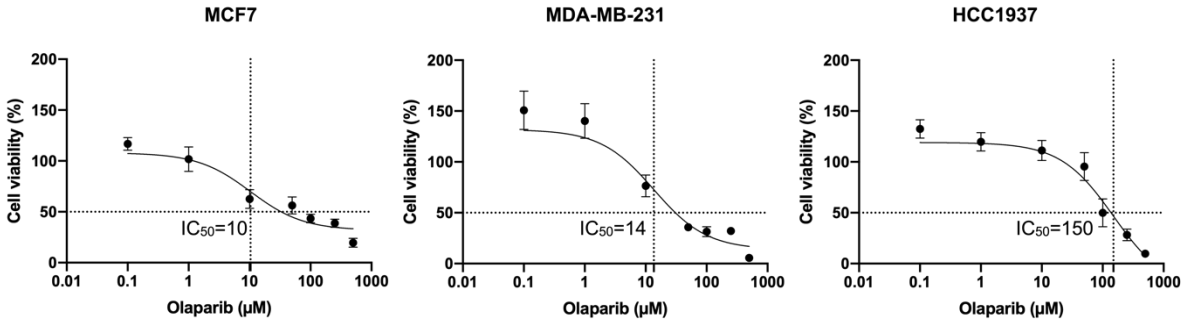

Figure 1 *Corresponding MTS dose-response curves for MCF7, HCC1937 and MDA-MB-231 cells treated with ascending doses of olaparib (0.1-500 μM) for seven days. The corresponding R^2 values for fitted dose-response curves in MCF7 (IC_{50}= 10 μM), MDA-MB-231 (IC_{50}= 14 μM), and HCC1937 (IC_{50}= 150 μM) cells were 0.89, 0.91 and 0.85, respectively.*

Our results show that exposure to olaparib caused a reduction in cell viability in all cell lines in a dose-dependent manner (**Figure 1**). We observed superior efficacy of olaparib in reducing cell viability in both MCF7 and MDA-MB-231 cells, with a calculated half maximal inhibitory concentration (IC_{50}) of 10 μM and 14 μM, respectively. However, in the case of HCC1937 cells, a higher concentration of olaparib was required to achieve the same reduction in cell viability (150 μM), indicating a lower efficacy of response to olaparib in this cell line.

Exposure to olaparib induces dose-dependent formation of γH2AX and 53BP1 foci in breast cancer cells

PARP inhibition induced by olaparib exposure results in the accumulation of DNA damage in cells by compromising their DDR mechanisms. Therefore, we next investigated the extent to which olaparib exposure at various doses (IC_{10}, IC_{25} and IC_{50}- determined from MTS assays) promotes the accumulation of DNA double strand breaks (DSBs) in MCF-7, MDA-MB-231 and HCC1937 cell lines. Key markers for DNA DSB formation include phosphorylated histone H2 variant H2AX (γH2AX) (19) and the damage sensor p53-binding protein 1 (p53BP1), which are rapidly recruited to sites of DNA damage and their accumulation is directly proportional to the number of DSB lesions (20). To measure the extent of DNA DSB formation, we performed immunofluorescence of phosphorylated 53BP1 foci and gamma-H2AX.

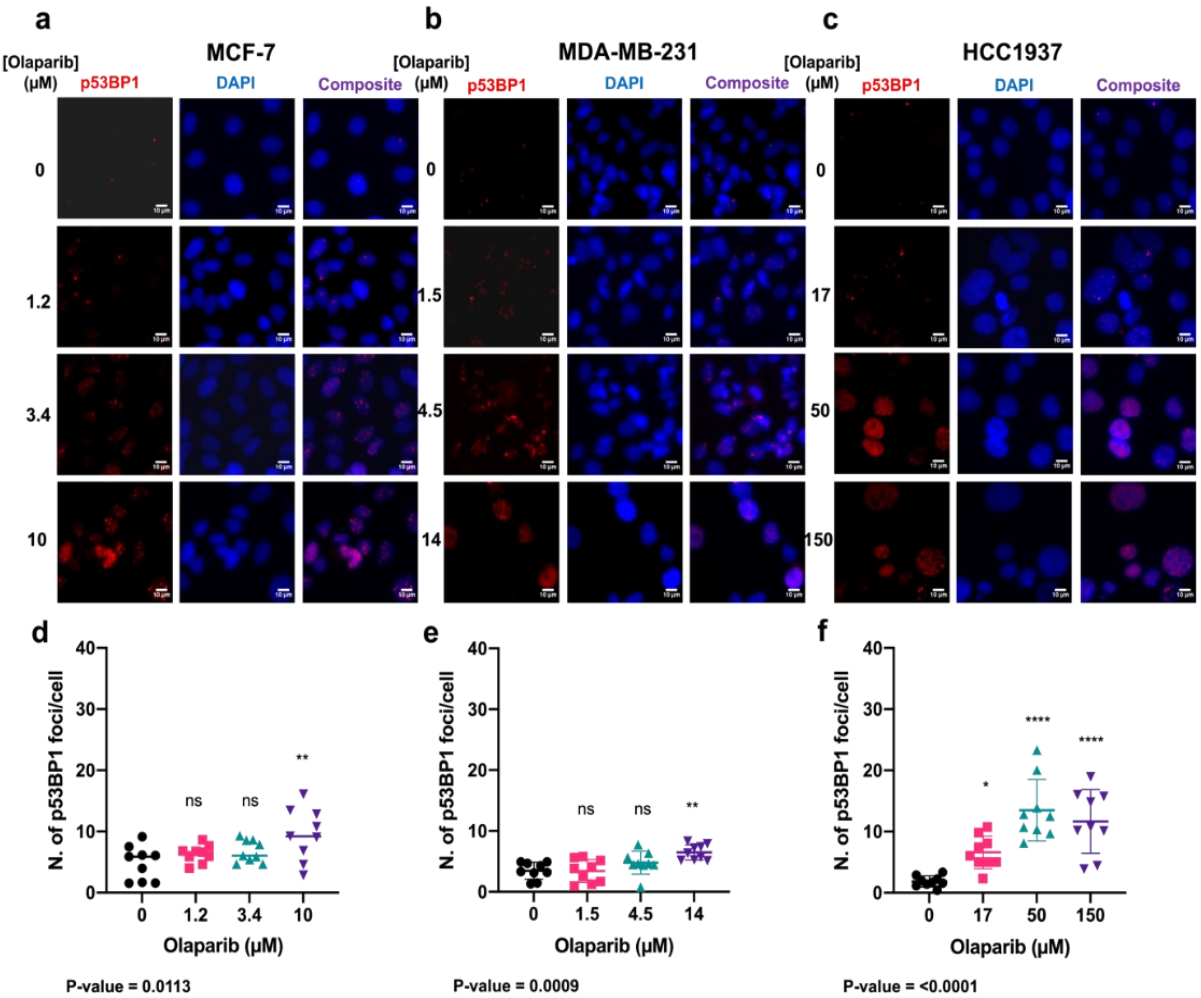

Figure 2 *The formation of p53BP1 foci in response to treatment with either growth medium or medium containing olaparib at various concentrations. Representative images of immunolabelled P53BP1 foci (red), DAPI (blue) nuclear counterstain and composite (p53BP1 (red) and DAPI (blue)) in MCF-7, MDA-MB-231, and HCC1937 cells treated with olaparib for seven days (a-c). Corresponding p53BP1 foci counts determined using Cell Profiler (d-f). 9 repeats with on average >100 cells per each sample. p-values have been determined through ANOVA test. Dunnett's multiple comparison test was used as a follow up to ANOVA test and the p-values were represented as: non-significant=ns, 0.05=*, 0.005=**, 0.0005=***, >0.00005=****.*

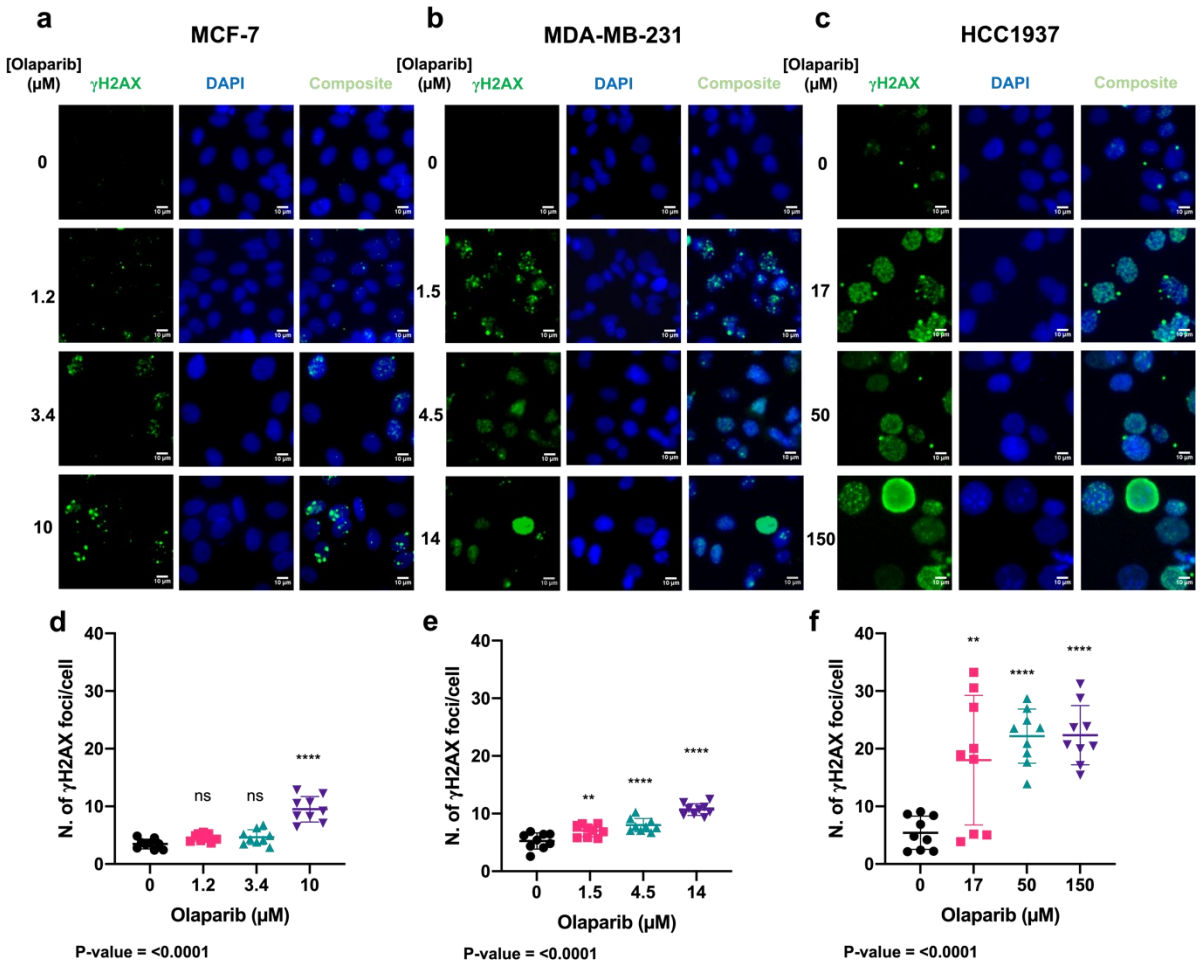

Figure 3 *The formation of γH2AX foci formation in response to treatment with either growth medium or medium containing olaparib at various concentrations. Representative images of immunolabelled γH2AX foci (green), DAPI (blue) nuclear counterstain and composite (γH2AX and DAPI) in MCF-7, MDA-MB-231, and HCC1937 cells treated with for seven days (a-c). Corresponding γH2AX foci counts determined using Cell Profiler (d-f). (>100 cells per sample). Dunnett's multiple comparison test was used as a follow up to ANOVA and corresponding p-values were represented as: non-significant=ns, 0.05=*, 0.005=**, 0.0005=***, >0.00005=****.*

Based on our results, p53BP1 and γH2AX foci levels increased in a dose-dependent manner in both MCF7 and MDA-MB-231 cells in response to ascending doses of olaparib (**Figure 2a,b,d,e**; **Figure 3a,b,d,e**). However, in HCC1937 cells, the expression of both markers was observed to decrease at the highest olaparib treatment dose (150 μM), in comparison to the 15 and 50 μM exposure doses (**Figure 2c,f**; **Figure 3c,f**). Generally, HCC1937 cells showed a higher number of both p53BP1 (mean >10 foci per cell) and γH2AX foci (mean > 20 foci per cell), compared to the MCF7 and MDA-MB-231 cells, where a mean of <10 foci per cell were measured for both markers. These results are consistent with the dose-dependent sensitivity of MCF7 and MDA-MB-231 cells in response to olaparib exposure, further confirming cell-line dependent response to olaparib exposure.

Biomolecular pathways altered in response to olaparib exposure vary across different cell lines

To comprehensively measure the extent of variation induced by olaparib exposure in MCF-7, MDA-MB-231 and HCC1937 cell lines, we profiled their metabolome using an in-house

untargeted liquid chromatography-mass spectrometry-based metabolomics pipeline. In **Figure 4** we describe the pipeline of the untargeted metabolomic study. After data acquisition, data processing and analysis were performed in Compound Discoverer 3.2. First, we used the principal component analysis (PCA) to visualise and interpret the clustering of quantified metabolite data to examine global differences between treatment groups and cell lines examined, which was followed by pairwise PCA analyses between control and treated groups across positive and negative analysis modes (**Figure 4**).

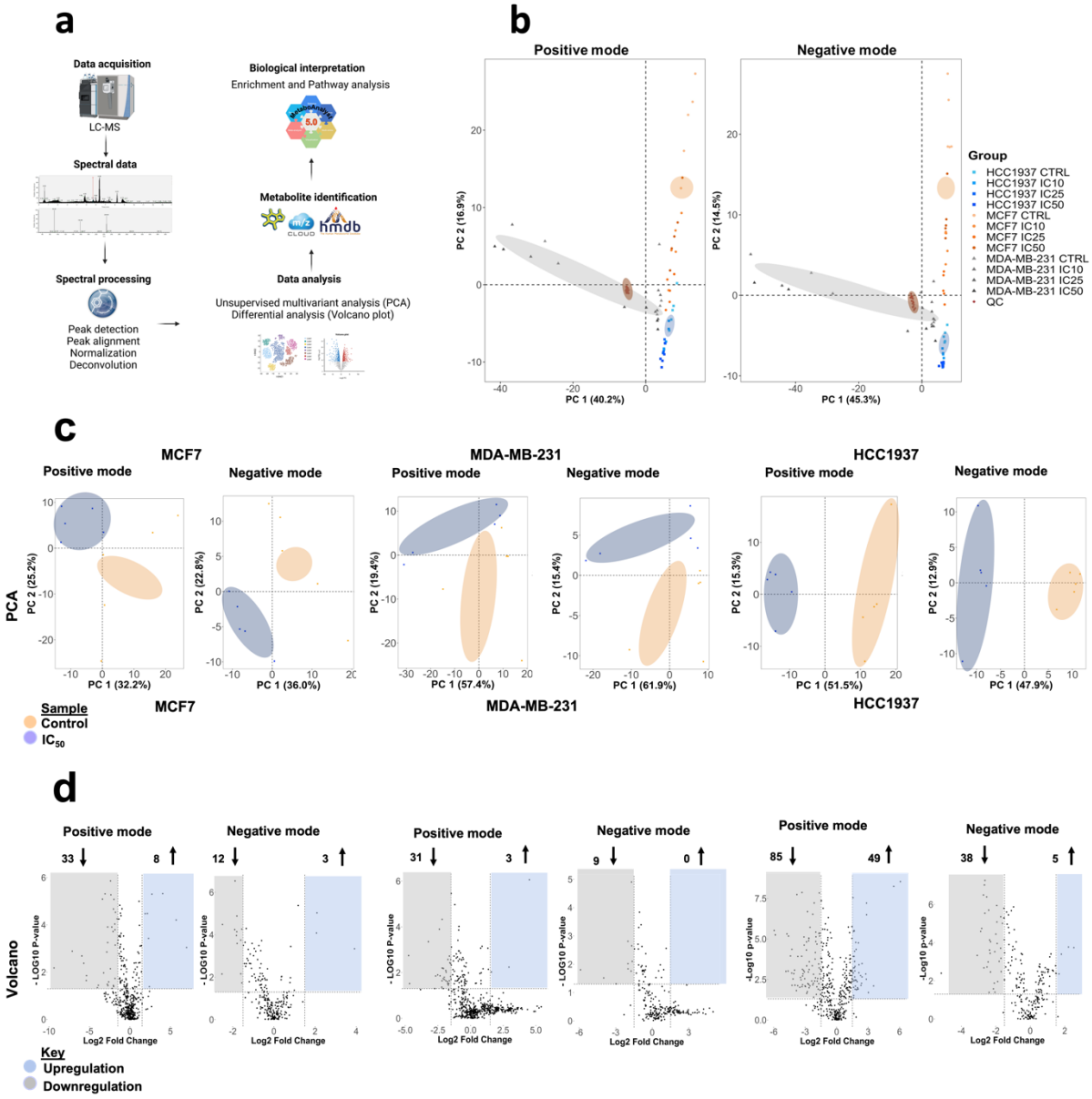

Figure 4 *Statistical analyses of global metabolic features identified in MCF7, MDA-MB-231 and HCC1937 upon exposure to IC_{10}, IC_{25} and IC_{50} olaparib doses for seven days acquired in positive and negative ionization mode. a) Workflow used in this study to perform pathway analysis from metabolomics analyses. b) Global PCA score plots of the analysed breast cancer cell lines for data acquired in positive and negative ionization mode. For each sample group, five replicates were used. Data points in the two-dimensional PCA score plot were central scaled. c) PCA pairwise analysis and differential analysis of metabolites altered in IC_{50}-treated cells, d) Volcano plots displaying upregulated (blue) and downregulated (grey) metabolic features by representing the log2 fold change in altered features and the -log10 adjusted p-values with cut off values selected at >1.5 and <0.05, respectively.*

Pooled quality control (QC) data confirm the stability of the data acquisition system across all the measurements performed in positive and negative ionization acquisition modes (**Figure 4 b**). Distinct clustering patterns were observed, with better separation for the IC_{50} olaparib treatment dose across all cell lines (**Figure 4 c**; **Figure S 1**). Volcano plots indicate the differential number of metabolic features that are significantly altered following exposure to olaparib, relative to control (**Figure 4 d**.; **Figure S 2**). From a metabolic perspective, we observed that HCC1937 (BRCA1-mutated) cells were the most susceptible to exposure at the IC_{50} olaparib treatment dose, while the MCF7 cells showed a higher number of significantly altered metabolic features at the IC_{25} olaparib treatment concentration (**Table S 2**). Together, these findings show a differential dose- and cell line- dependent metabolic response to olaparib exposure.

Amino acid and lipid metabolism are significantly altered in response to olaparib exposure

To analyse specific biomolecular pathways altered by olaparib exposure, we used MetaboAnalyst to identify key metabolic pathways significantly perturbed by olaparib treatment, and performed enrichment analysis for both control and treated samples (**Figure 5**, **Figure S 3**). Among the enriched pathways ranked in the top ten, we selected altered pathways with a corresponding pathway impact >0.1, and a p-value <0.05. (**Table S 3a,b**).

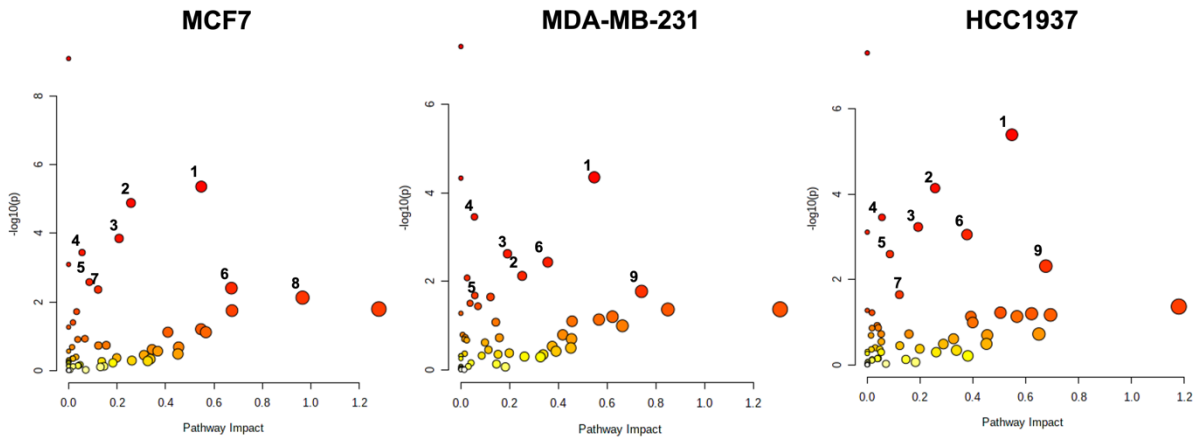

Figure 5 *Pathway enrichment analysis of MCF7 (10 μM), MDA-MB-231 (14 μM) and HCC1937 (150 μM) cells following a seven-day exposure to olaparib. Enrichment analysis was based on the hypergeometric test. Topological analysis was based on betweenness centrality. The tight integration method was used by combining genes and metabolites into a single query. A p<0.05, and pathway impact >0.1 were deemed significant.*

Across all cell lines examined, the top ten putative pathways significantly altered in Metaboanalyst (**see Figure 5**) were based on amino acid (arginine biosynthesis, glutamine, glycine, serine and threonine metabolism) and lipid metabolism (butanoate metabolism). Following the identification of metabolic pathways altered by olaparib exposure, we constructed a Venn diagram (**Figure S 4**) to outline common overlapping and cell line-specific altered metabolic features.

Overlapping enriched pathways are mostly represented by amino acid metabolism (glutamine, glutamate, aspartate, alanine, arginine and proline), suggesting a strong reliance of breast cancer cell metabolism on amino acids under baseline conditions (control samples). Upon olaparib exposure, the same pathways (amino acid metabolism) were among the most significantly-altered across all cell lines, while fatty acid (butanoate metabolism) and vitamin B6 metabolism were only significantly perturbed in MCF-7 cells.

Next, we explored individual metabolites that were associated with significantly altered metabolic pathways in response to olaparib exposure and evaluated relative changes in their levels between control and treatment samples. These results are presented through a heatmap clustering analysis (**Figure 7**). A correlation analysis between each metabolite is shown in **Figure S 4**, and a wider list of compounds specific for each cell type is provided in **Supplementary Table 4**.

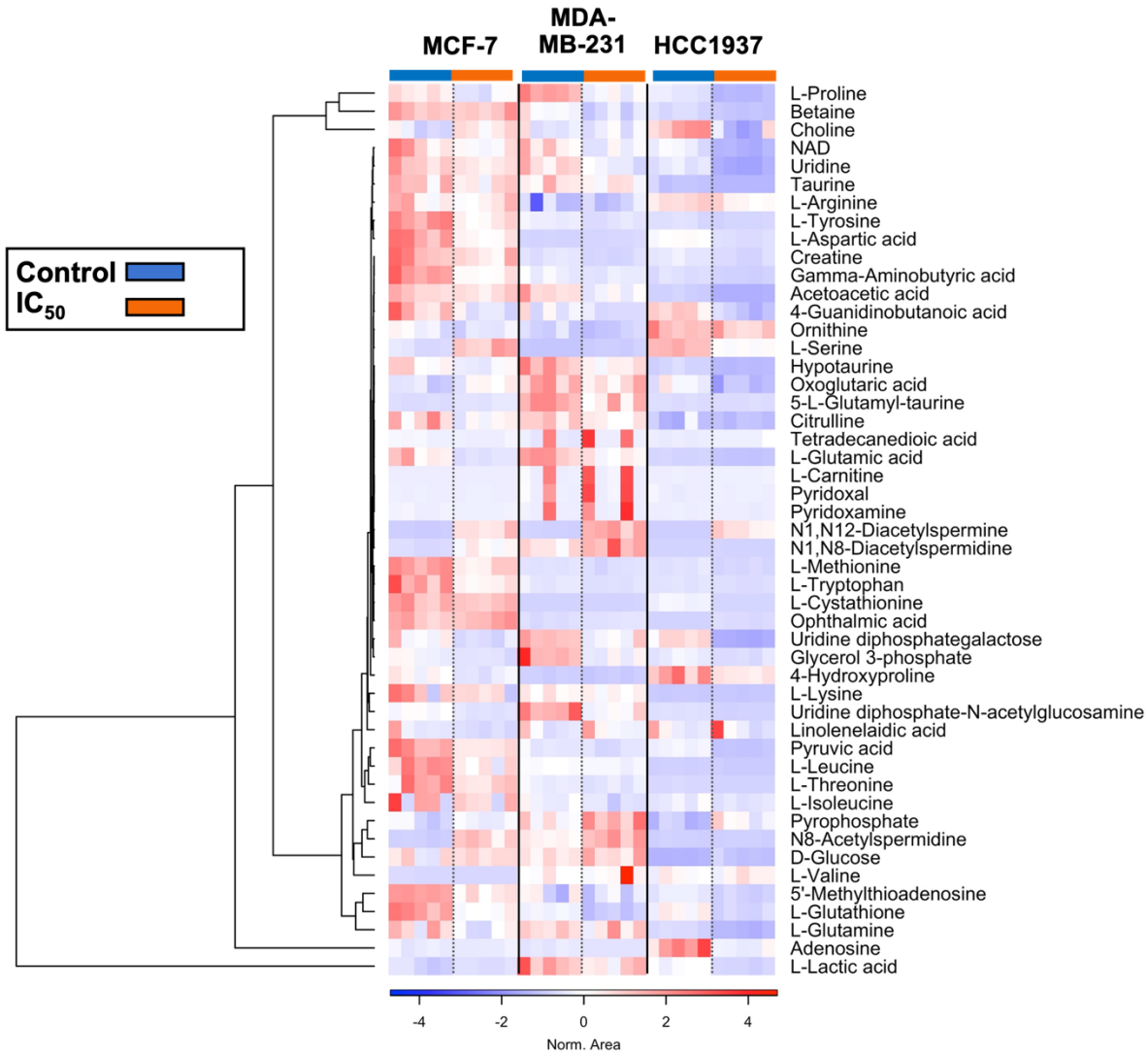

Figure 7 *Heatmap cluster analysis of relevant metabolites associated with the pathways altered upon exposure to olaparib in MCF7 (10 μM), MDA-MB-231 (14 μM) and HCC1937 (150 μM) cells for seven days. Clustering and distance function are Ward and Euclidean, respectively. Normalised areas indicate chromatographic peaks areas that have been normalised based on the QC samples in order to compensate for batch effects.*

Multiple amino acids (glutamine, glutamate, arginine, proline, methionine, glycine, threonine, taurine, and hypotaurine) were found to be downregulated following olaparib exposure (relative to control) in all cell lines examined. An overview of their chemical properties is given in **Supplementary Table 5**. Arginine and proline metabolism were significantly downregulated by olaparib exposure, with downregulation of their derived polyamines detected in all cell lines examined. Conversely, catabolic products of arginine and proline metabolism (N8-Acetylspermidine, N1-N8-Diacetylspermidine, and N1-N12-Diacetylspermine) were upregulated. Elevated levels of serine were observed in MCF7 and MDA-MB-231 cells, while downregulation of serine was detected in the HCC1937 cells.

Alpha-ketoglutarate (α-KG- glutamine-derived intermediate of the TCA cycle), was upregulated in MCF7 and downregulated in MDA-MB-231 and HCC1937 cells. A negative correlation was observed between α-KG and glutamine levels, and a positive correlation between α-KG, and citric and fumaric acid (TCA cycle intermediates). Aspartate (a TCA cycle product), accumulated in the KRAS-mutant MDA-MB-231 cells, while aspartate downregulation was observed in MCF7 and HCC1937 cells. Glucose levels were found to be significantly elevated relative to control samples in HCC1937 cells. Asparagine (a byproduct of aspartate) was absent in MDA-MB-231 cells, while its accumulation was detected in MCF7 and HCC1937 cells. In parallel, accumulation of AMP was observed in both MCF7 and HCC1937 cell lines, while it was absent in MDA-MB-231 cells and accumulation of PPi was detected in all cell lines examined following olaparib exposure.

In the case of lipid metabolism, we observed a global downregulation of phosphocholines (PC) and phosphoethanolamines (PE) in all cell lines following olaparib treatment. Acylcarnitine levels varied across the cell lines, with an overall upregulation of long (C14 – C21) and very-long chain acylcarnitines (>C22) in all cell lines treated with olaparib. Moreover, we observed elevated alpha-linoleic acid (a polyunsaturated fatty acid-PUFA) levels in MCF7 and MDA-MB-231 cells, which was absent in HCC1937 cells.

Other metabolites included in the enrichment study – which did not emerge as significantly altered- were implicated in glucose and nucleotide metabolism. Compared to non-treated cells, elevated levels of glucose were detected in all the cell lines upon treatment with olaparib, while downregulation of most nucleobases was observed. Finally, NAD+ downregulation was detected in all cell lines treated with olaparib.

An overview of the metabolic features altered in response to olaparib exposure is given in **Figure 8**. We mapped cell line differences in metabolite levels through the Kyoto Encyclopaedia of Genes and Genomes (KEGG) database.

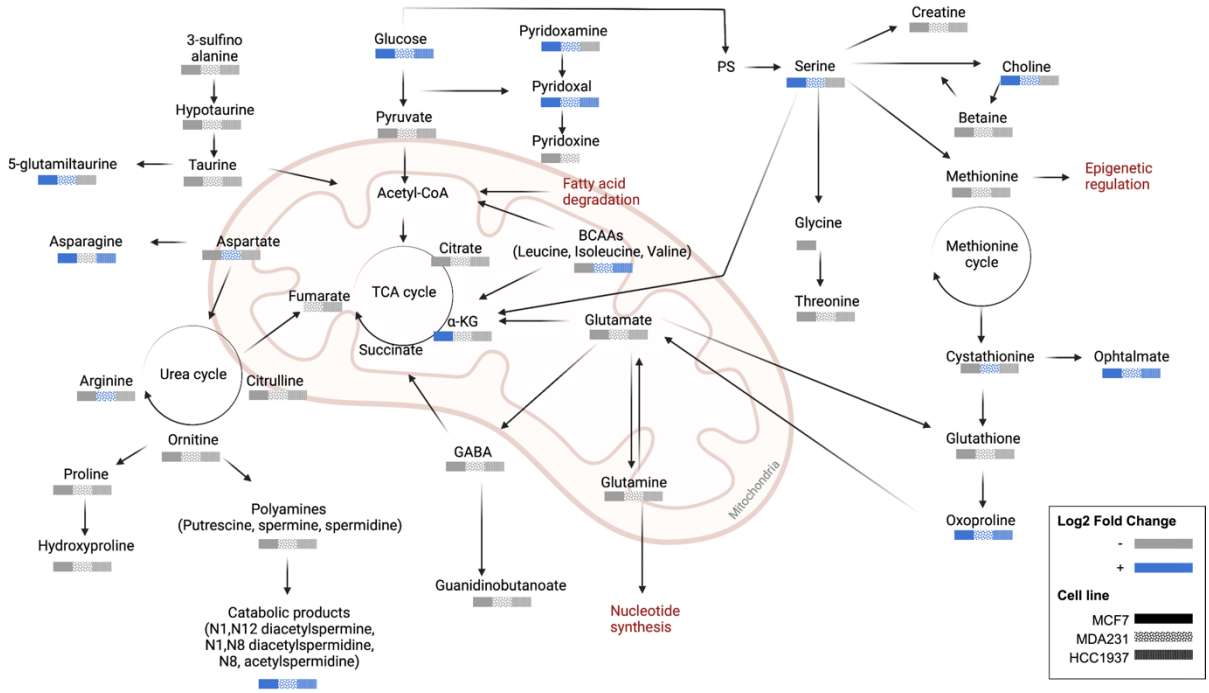

Figure 8 *A summary of putatively identified metabolic pathways altered in response to olaparib exposure. Significantly altered features with a Log2 fold change of >1.5 (blue-upregulated and grey-downregulated). MCF-7 (▬), MDA-MB-231 (▬), and HCC1937 (▬).*

DISCUSSION

PARP inhibitors have shown promising results in the treatment of metastatic breast cancers harbouring germline BRCA1/2 mutations (21,22). Recent clinical studies have shown evidence of PARP inhibitor efficacy in the management of breast cancer, irrespective of tumour BRCAness. Prior work has shown that BRCA1-mutated cells carrying a TP53 mutation are resistant to treatment with PARP inhibitors (23). Therefore, additional factors beyond BRCAness may govern sensitivity to PARP inhibition.

In this study we analyzed the sensitivity of two triple-negative (MDA-MB-231 and HCC1937) and MCF-7 (ER+, PR-, HER2-) cell lines to olaparib PARP inhibition (PARP1/2). The rationale for selecting these cell lines was to explore how their different genetic profiles define the observed differential biomolecular perturbations in response to olaparib treatment. Initially, we examined the responsiveness of MCF-7, MDA-MB-231 and HCC1937 cell lines to olaparib exposure using the MTS cell viability assay (**Figure 1**). Our results showed differential sensitivity to olaparib exposure across the cell lines examined, with MCF-7 and MDA-MB-231 showing sensitivity to olaparib treatment at lower micromolar concentrations, and the BRCA1-mutant HCC1937 cell line showing less sensitivity (IC_{50}- 150 μM). These findings are in agreement with previous reports of HCC1937 resistance to PARP inhibition, where the identification of predictive biomarkers of response to PARP inhibitor treatments was recommended beyond BRCA1/2 status (23).

Our analysis of γH2AX and 53BP1 DNA DSB immunolabelled foci (**Figure 3**) showed a higher occurrence of DNA damage foci in HCC1937 cells in comparison with MCF-7 and MDA-MB-231 cells with wild-type BRCA status. These observations suggest that BRCA status does not necessarily translate to olaparib sensitivity, and additional DDR components may define responsiveness. At present, routine clinical decision making surrounding the selection of treatment interventions are based on BRCA status, anatomical location, hormone receptor status and tumour stage, with very limited attention given to other mediators of DDR- namely homologous recombination- known to confer a BRCAness phenotype similar to BRCA 1 or 2 loss. Several recent studies have used whole-genome sequencing or the integration of homologous recombination panel scoring systems to provide an additional framework for predicting responders to PARP inhibitor treatment (24,25).

Genetic biomarkers are routinely used in the clinical stratification of breast cancers and predicting treatment-emergent resistance (26). While genome-wide studies have improved patient stratification efforts, they lack the potential to account for functional phenotypic effects resulting from protein expression levels, or gain- or loss of function effects. Metabolomics has emerged in the past decade as an additional research toolbox for studying potential biomarkers of breast cancer with a range of applications ranging from early detection to the discovery of new metabolites and prognostic classification of patients with breast cancer (27).

Our goal in the present study was to apply combined analysis of DNA damage foci formation with global untargeted mass-spectrometry based metabolomics to map the metabolic changes occurring following exposure to olaparib. We examined the baseline differences in cellular metabolism across the cell line panel and extended this evaluation to examine cell line dependent response to olaparib treatment. Under baseline cell culture conditions, we found overlapping metabolic features (alanine, aspartate, glutamine, arginine, proline, glycine, serine, and threonine) occurring across all three breast cancer cell lines studies, and metabolic signatures that were unique to specific cell lines (MCF7: sphingolipid and glycerophospholipid metabolism; MDA-MB-231: taurine and hypotaurine metabolism; HCC1937: glyoxylate and dicarboxylate metabolism) (**Figure 5-6**).

Our analysis of metabolites significantly altered in response to olaparib treatment correlate with reports from Bhute *et al*, where metabolic markers of PARP inhibition were reported as

changes in amino acid metabolism (glutamine and alanine), downregulation of osmolyte levels (taurine, and GPC), phosphocreatine, lactate and pyruvate in MCF7 cells (28). We reported downregulation of those metabolites also in the MDA-MB-231 and HCC1937 cells, while low levels of fumarate were observed only in the HCC1937 cells (**Figure 7, supplementary Table 4**). Bhute *et al.* also reported increased NAD+ levels for cells treated with veliparib. In our results NAD+ levels increased in the MCF7 cells treated with olaparib at the IC_{10} treatment concentration, accompanied by a decrease in NAD+ levels at ascending concentrations of olaparib. Reduced levels of NAD+ were also detected in the MDA-MB-231 and HCC1937 cells at all treatment concentrations. Recent studies have shown that in TNBC cells, olaparib enhances the signalling pathways of other NAD+-dependent deacetylase (i.e., sirtuins) (28, 29). These findings are in agreement with our observation of downregulation of acetyl-amino acids and upregulation of methyl-pyridines, -pyrrolidines, and -nucleosides (**supplementary Table 4**). Further studies are needed to confirm the divergence of NAD+ flow towards alternative pathways and its association with specific breast cancer subphenotypes.

Glutamine- a precursor for protein, nucleotide, and lipid biosynthesis- is a fundamental amino acid in breast cancer cell metabolism, playing a pivotal role in providing anaplerotic intermediates for the tricarboxylic acid (TCA) cycle (30). Previous reports have indicated a reduction of glutamine levels only for the TNBC cells after treatment with veliparib, and in the MCF7 cells only in combination with other DNA damage repair agents (16,28). Our results show reduced glutamine levels in all cell lines treated with olaparib, suggesting increased glutamine utilisation. Once internalised by cells, glutamine can be converted to glutamate and alpha-ketoglutarate (α-KG). α-KG- also a by-product of isocitrate- is oxidised in the TCA cycle through a reaction catalysed by isocitrate dehydrogenase (IDH), which is frequently mutated in cancer. Several studies have studied α-KG as an oncometabolite, where elevated levels induce the reversal of enhanced glycolysis through downregulation of the Hypoxia-inducible factor (HIF1), which following PARP inhibition leads to cell death (31,32). Recent findings have shown that mutant IDH - and the consequent synthesis of aberrant α-KG forms - confers a BRCAness phenotype (33), downregulating the expression of the DNA repair enzyme Ataxia-telangiectasia mutated (ATM) kinase (34), altering the methylation status of loci surrounding DNA breaks (35). Together, these alterations lead to homology-dependent repair (HDR) impairment and increase susceptibility to PARP inhibition. On this basis, the reduced α-KG levels observed in olaparib-treated MDA-MB-231 and HCC1937 cells shows the basis for potential resistance to the anti-proliferative effects of olaparib. The increased utilisation of α-KG by HCC1937 cells, is paralleled by an increased consumption of serine at ascending doses of olaparib (**supplementary table 4**). These observations are consistent with reports that in BRCA1-mutated TNBC cell lines, approximately 50% of α-KG results from the flux of serine metabolism (36).

Glutamine is also a source of nitrogen groups for the synthesis of nucleobases and nucleotides, either directly or through a process involving the transamination of glutamate and the TCA cycle-derived oxaloacetate that generates aspartate (37-39). Our results show low levels of glutamine are associated with overall reduction in nucleobase and nucleotide levels. MCF7 and HCC1937 cells showed accumulation of adenosine monophosphate (AMP), which represents a depleted energy and nutrient status of the cells known to activate the metabolic sensor AMP-activated protein kinase (AMPK) leading to cell growth inhibition (40). Different studies have considered activation of AMPK a metabolic cancer suppressor and an attractive therapeutic target for TNBC (41), however, its signalling network in response to PARP inhibition in different breast cancer cells needs to be established. Opposite to what observed by Bhute *et al*, Aspartate, a byproduct of the TCA cycle, accumulated in the MDA-MB-231 cells after PARP inhibition compared to its reduction in the MCF7 and HC1937 cells. Lowered plasma aspartate levels have been diagnosed in breast cancer patients suggesting an increased tumour utilisation of this metabolite (42). Moreover, we observed that aspartate metabolism is relevant both in the baseline model and in response to olaparib, which suggests a role of this metabolite in regulating the different metabolic phenotypes of breast cancer cells.

However, its role has been poorly investigated and little is known about its association with PARP inhibition.
Among the pathways of aspartate utilisation, asparagine is converted through the enzyme asparagine synthetase (ASNS). The reaction requires glutamine as a substrate and consumption of adenosine triphosphate (ATP) to produce adenosine monophosphate (AMP) and pyrophosphate (PPi). Physiological levels of asparagine occur at levels of <0.05 mM in human plasma (44). Cancer cells harbouring mutant KRAS (e.g. MDA-MB-231), possess lower ASNS expression levels, leading to lower baseline aspartate levels explaining the rationale for the lack of aspartate detection in MDA-MB-231 lines (45). In breast cancer cells the increased bioavailability of asparagine promotes metastatic progression (45), due to its role in protein synthesis and regulation of amino acid homeostasis (46). We found elevated asparagine levels in olaparib-treated MCF7 and HCC1937 cells, suggesting a role for asparagine in the observed responses to exposure to PARP inhibitor.

Beyond asparagine synthesis, aspartate amidation through ASNS presents a source of amino building blocks for the synthesis of arginine in the urea cycle, which is in turn responsible for the synthesis of polyamines catalysed by ornithine decarboxylase (ODC). Polyamine accumulation previously has been correlated with the increased proliferation of both hormone-dependent and independent breast cancer cells (47), and recently found to contribute to BRCA1-mediated DNA repair (48). Moreover, metabolic profiling of plasma samples from patients with TNBC revealed an increase of diacetyl spermines associated with elevated expression of MYC, a well-known oncogene driving TNBC development and proliferation. Here, we found elevated diacetyl spermine levels following olaparib treatment in both TNBC and non-TNBC cells, suggesting an upregulation of polyamine catabolism, irrespective of cell line BRCA- and hormone receptor- status. Parallel to their relevance in cellular metabolism, amino acids serve also as biological buffers through regulation of cellular pH. Low extracellular pH is associated with positively charged amino acids and a known hallmark of cancer arising from enhanced glycolysis, production and altered lactate metabolism, resulting in altered mTOR pathway activation, ultimately regulating cancer cell metabolism (49, 50).

Glutathione (GSH) is involved in the protection against ROS and regulation of intracellular redox homeostasis. Elevated GSH levels have previously been reported in TNBC compared to luminal breast cancers, suggesting the relevance of GSH to our observations of lower sensitivity to olaparib in TNBC cell lines (17,51).

Lipids mediate various cellular biological functions, including energy storage, cell membrane structural composition and signal transduction, the increased biosynthesis of which is a marker of metabolic rewiring observed in malignant breast cancers (52,53). Our findings show downregulation of fatty acid biosynthesis following olaparib treatment, with a reduction in phospholipid levels including lysophosphatidylcholines and glycerolphosphocholines in all cell lines (**supplementary Table 4**). Poly-unsaturated fatty acids (PUFAs), have previously been implicated in MCF7 and MDA-MB-231 cell apoptosis through the induction of lipid peroxidation and altered cellular redox state (54). Moreover, elevated PUFA levels have been associated with the proteolytic cleavage of PARP and its inhibition, leading to cell death (55). On this basis, the reduced PUFA levels observed in HCC1937 cells may indicate their resistance to olaparib treatment. Only a limited number of studies have reported a correlation between PUFAs and breast cancer subphenotypes, requiring further validation by additional studies.

Future targeted metabolomics studies using additional TNBC cell lines and clinical tumour clinical specimens are required to validate our observations. Validation of our findings could define prognostic biomarkers that will aid diagnose and enable the implementation of precision medicine in the management of breast cancer.

CONCLUSION

Our data show differential sensitivity of breast cancer cell lines to olaparib treatment that was dose-dependent and demonstrated the increased sensitivity of TNBC cells to DNA damage foci accumulation. The application of metabolomics to the study of breast cancer remains in its infancy, with only a handful of studies reporting combined metabolomics and phenotypic analyses. Data acquired from metabolomics analysis can be validated against routine molecular biology and phenotypic assays, providing a powerful platform for biomarker detection or the discovery of novel actionable pathways for drug development.

Our results show that fingerprinting the metabolic profile of cells can be a powerful tool for uncovering potential oncometabolites or mechanisms giving rise to chemoresistance. Findings from such studies may provide potential additional actionable targets for modulating response to drug treatment or the design of new drug combinations that will overall enhance DNA damage efficacy, ultimately improving patient response to radiotherapy and adjuvant chemotherapy.

ACKNOWLEDGEMENTS

The authors acknowledge funding of these studies from Tenovus Scotland and the Royal Society of Edinburgh Research Reboot funding. We acknowledge support from the Strathclyde Centre for Molecular Biology (SCMB) for providing access to mass spectrometry facilities. ZR acknowledges funding from the UK Engineering and Physical Sciences Research Council (EPSRC- EP/V028960/1).

AUTHOR CONTRIBUTIONS

Conceptualization: ZR, NJWR, and DB.; Investigation: DB, YH, GF, NJWR, ZR.; Methodology: DB, YH, LvDD, GF, ZR, NJWR.; Analysis: DB, YH, NJWR, ZR, LvDD.; Writing original draft: ZR and DB.; Visualization: DB, LvDD, NJWR, ZR.; Writing- reviewing and editing: DB, YH, LvDD, GF, NJWR, ZR.; Funding acquisition: NJWR and ZR. All authors have read and agreed to the published version of the manuscript.

DATA AVAILABILITY STATEMENT

The datasets generated and used/or analysed are available from the corresponding authors upon request.

CONFLICTS OF INTEREST

The authors declare no conflict of interest.

REFERENCES

1. 1. Gueble SE, Bindra RS. Oncometabolites as Regulators of DNA Damage Response and Repair. Seminars in Radiation Oncology **2022**;32:82-94
2. Huang R, Zhou P-K, et al. DNA damage repair: historical perspectives, mechanistic pathways and clinical translation for targeted cancer therapy. Signal Transduction and Targeted Therapy **2021**;6:254
3. He C, Kawaguchi K, Toi M. DNA damage repair functions and targeted treatment in breast cancer. Breast cancer (Tokyo, Japan) **2020**;27:355-62
4. Rizzolo P, Silvestri V, Falchetti M, Ottini L. Inherited and acquired alterations in development of breast cancer. The application of clinical genetics **2011**;4:145-58
5. Godet I, Gilkes DM. BRCA1 and BRCA2 mutations and treatment strategies for breast cancer. Integrative Cancer Science and Therapeutics **2017**;4:10.15761/ICST.1000228
6. O'Neil NJ, Bailey ML, Hieter P. Synthetic lethality and cancer. Nature Reviews Genetics **2017**;18:613-23

7. Li S, Topatana W, Juengpanich S, Cao J, Hu J, Zhang B*, et al.* Development of synthetic lethality in cancer: molecular and cellular classification. Signal Transduction and Targeted Therapy **2020**;5:241
8. Lord CJ, Tutt ANJ, Ashworth A. Synthetic Lethality and Cancer Therapy: Lessons Learned from the Development of PARP Inhibitors. Annual Review of Medicine **2015**;66:455-70
9. Cortesi L, Rugo HS, Jackisch C. An Overview of PARP Inhibitors for the Treatment of Breast Cancer. Targeted Oncology **2021**;16:255-82
10. Food and Drug Administration. FDA approves olaparib for adjuvant treatment of high-risk early breast cancer. 2022.
11. Pavlova, NN, Thompson CB. The Emerging Hallmarks of Cancer Metabolism. Cell Metabolism **2016**;27-47
12. Maria RM, Altei WF, Selistre-de-Arujo HS, Colnago LA. Impact of chemotherapy on metabolic reprogramming: Characterization of the metabolic profile of breast cancer MDA-MB-231 cells using 1H HR-MAS NMR spectroscopy. Journal of Pharmaceutical and Biomedical Analysis **2017**;146:324-8
13. Gandhi N, Das GM. Metabolic Reprogramming in Breast Cancer and Its Therapeutic Implications. Cells **2019**;8
14. Palaskas N, Larson SM, Schultz N, Komisopoulou E, Wong J, Rohle D, Campos C, Yannuzzi N, Osborne JR, Linkov I, Kastenhuber ER, et al. 18F-fluorodeoxy-glucose positron emission tomography marks MYC-overexpressing human basal-like breast cancers. Cancer Research **2011**;71:5164-74
15. Turgeon MO, Perry NJS, Poulogiannis G. DNA Damage, Repair, and Cancer Metabolism. Frontiers in Oncology **2018**;8:1-8
16. Bhute VJ, Ma Y, Bao X, and Paleceka SP. The Poly (ADP-Ribose) Polymerase Inhibitor Veliparib and Radiation Cause Significant Cell Line Dependent Metabolic Changes in Breast Cancer Cells. Scientific Reports **2016**;6
17. Tang X, Lin CC, Spasojevic I, Iversen ES, et al. A joint analysis of metabolomics and genetics of breast cancer. Breast Cancer Research **2014**;16
18. Huang A, Garraway LA, Ashworth A, Weber B. Synthetic lethality as an engine for cancer drug target discovery. Nature Reviews Drug Discovery **2020**;19:23-38
19. Mah LJ, El-Osta A, Karagiannis TC. γH2AX: a sensitive molecular marker of DNA damage and repair. Leukemia **2010**;24:679-86
20. Schultz LB, Chehab NH, Malikzay A, Halazonetis TD. p53 binding protein 1 (53BP1) is an early participant in the cellular response to DNA double-strand breaks. The Journal of Cell Biology **2000**;151:1381-90
21. Robson M, Im SA, Senkus E, Xu B, et al. Olaparib for Metastatic Breast Cancer in Patients with a Germline BRCA Mutation. New England Journal of Medicine **2017**;377:523-33
22. AstraZeneca. 2022 04/2022. Lynparza approved in the US as adjuvant treatment for patients with germline BRCA-mutated HER2-negative high-risk early breast cancer. <https://www.astrazeneca.com/media-centre/press-releases/2022/lynparza-approved-in-the-us-as-adjuvant-treatment-for-patients-with-germline-brca-mutated-her2-negative-high-risk-early-breast-cancer.html>. 04/2022.
23. Keung MY, Wu Y, Badar F, and Vadgama JV. Response of Breast Cancer Cells to PARP Inhibitors Is Independent of BRCA Status. Journal of Clinical Medicine **2020**;9:940
24. Davies H, Glodzik D, Morganella S, Yates LR, Staaf J, Zou X*, et al.* HRDetect is a predictor of BRCA1 and BRCA2 deficiency based on mutational signatures. Nature Medicine **2017**;23:517-25
25. McGrail DJ, Lin CC-J, Garnett J, Liu Q, Mo W, Dai H*, et al.* Improved prediction of PARP inhibitor response and identification of synergizing agents through use of a novel gene expression signature generation algorithm. Systems Biology and Applications **2017**;3:8

26. Harbeck N, Penault-Llorca F, Cortes J, Gnant M, Houssami N, Poortmans P*, et al.* Breast cancer. Nature Reviews Disease Primers **2019**;5:66
27. Hart CD, Tenori L, Luchinat C, Di Leo A. Metabolomics in Breast Cancer: Current Status and Perspectives. Advances in experimental medicine and biology **2016**;882:217-34
28. Bhute VJ, Palecek SP. Metabolic responses induced by DNA damage and poly (ADP-ribose) polymerase (PARP) inhibition in MCF-7 cells. Metabolomics **2015**;6:1779-91
29. Gajan A, Sarma A, Kim S, Gurdziel K, et al. Analysis of Adaptive Olaparib Resistance Effects on Cisplatin Sensitivity in Triple Negative Breast Cancer Cells. Frontiers in Oncology **2021**;11:1-14
30. Najumudeen AK, Ceteci F, Fey SK, Hamm G, et al. The amino acid transporter SLC7A5 is required for efficient growth of KRAS-mutant colorectal cancer. Nature Genetics **2021**;53:16-26
31. Tennant DA, Frezza C, MacKenzie ED, Nguyen QD, et al. Reactivating HIF prolyl hydroxylases under hypoxia results in metabolic catastrophe and cell death. Oncogene **2009**;28:4009-21
32. Scalia M, Satriano C, Greca R, Stella AMG, et al. PARP-1 Inhibitors DPQ and PJ-34 Negatively Modulate Proinflammatory Commitment of Human Glioblastoma Cells. Neurochemical Research **2013**;38:50-8
33. Sulkowski PL, Corso CD, Robinson ND, Scanlon SE, et al. 2-Hydroxyglutarate produced by neomorphic IDH mutations suppresses homologous recombination and induces PARP inhibitor sensitivity. Science Translational Medicine **2017**;9
34. Inoue S, Li WY, Tseng A, Beerman I, et al. Mutant IDH1 Downregulates ATM and Alters DNA Repair and Sensitivity to DNA Damage Independent of TET2. Cancer Cell **2016**;30:337-48
35. Sulkowski PL, Oeck S, Dow J, Economos NG, et al. Oncometabolites suppress DNA repair by disrupting local chromatin signalling. Nature **2020**;582:586-91
36. Possemato R, Marks KM, Shaul YD, Pacold ME, et al. Functional genomics reveal that the serine synthesis pathway is essential in breast cancer. Nature **2011**;476:346-50
37. DeBerardinis RJ, Cheng T. Q's next: the diverse functions of glutamine in metabolism, cell biology and cancer. Oncogene **2010**;29:313-24
38. Okazaki A, Gameiro PA, Christodoulou D, Laviollette L, et al. Glutaminase and poly(ADP-ribose) polymerase inhibitors suppress pyrimidine synthesis and VHL-deficient renal cancers. Journal of Clinical Investigation **2017**;127:1631-45
39. Son J, Lyssiotis CA, Ying H, Wang X, et al. Glutamine supports pancreatic cancer growth through a KRAS-regulated metabolic pathway. Nature **2013**;496:101-5
40. Hoyer-Hansen M, Jaattela M. AMP-activated protein kinase: a universal regulator of autophagy? Autophagy **2007**;3:381-3
41. Cao W, Li J, Hao Q, Vadgama JV, et al. AMP-activated protein kinase: a potential therapeutic target for triple-negative breast cancer. Breast Cancer Research **2019**;21
42. Xie G, Zhou B, Zhao A, Qiu Y, et al. Lowered circulating aspartate is a metabolic feature of human breast cancer. Oncotarget **2015**;6:33369-81
43. Stegink LD, Filer LJ, Brummel MC, Baker GL, et al. Plasma amino acid concentrations and amino acid ratios in normal adults and adults heterozygous for phenylketonuria ingesting a hamburger and milk shake meal. American Journal of Clinical Nutrition **1991**;53:670-5
44. Gwinn DM, Lee AG, Briones-Martin-Del-Campo M, Conn CS, et al. Oncogenic KRAS regulates amino acid homeostasis and asparagine biosynthesis via ATF4 and alters sensitivity to L-asparaginase. Cancer Cell **2018**;33:91-107
45. Knott SRV, Wagenblast E, Khan S, Kim SY, et al. Asparagine bioavailability governs metastasis in a model of breast cancer. Nature **2018**;554:378-81
46. Krall AS, Xu S, Graeber TG, Braas D, et al. Asparagine promotes cancer cell proliferation through use as an amino acid exchange factor. Nature Communications **2016**;7

47. Kim I, Lynch AMJ, Demers L. Polyamine involvement in the growth of hormone-responsive and -resistant human breast cancer cells in culture. Cancer Research **1989**;49:1371-6
48. Lee CY, Su GC, Huang WY, Ko MY, et al. Promotion of homology-directed DNA repair by polyamines. Nature Communication **2019**;10
49. Zhang X, Lin Y, Gillies RJ. Tumor pH and Its Measurement. Journal of Nuclear Medicine **2010**;51:1167-70
50. Balgi AD, Diering GH, Donohue E, Lam KKY*, et al.* Regulation of mTORC1 Signaling by pH. PLOS ONE **2011**;6:e21549
51. Lien EC, Lyssiotis CA,Juvekar A, Hu H, et al. Glutathione biosynthesis is a metabolic vulnerability in PI3K/Akt-driven breast cancer. Nat Cell Biol **2016**;18:572-8
52. Beckonert O, Monnerjahm J, Bonk U, Leibfritz D. Visualizing metabolic changes in breast-cancer tissue using 1H-NMR spectroscopy and self-organizing maps. NMR in Biomedicine **2003**;16:1-11
53. Cao MD, Dopkens M, Krishnamachary B, Vesuna F, et al. Glycerophosphodiester phosphodiesterase domain containing 5 (GDPD5) expression correlates with malignant choline phospholipid metabolite profiles in human breast cancer. NMR in Biomedicine **2012**;25:1033-42
54. Deshpande R, Mansara P, Suryavanshi S, Kaul-Ghanekar R. Alpha-linolenic acid regulates the growth of breast and cervical cancercell lines through regulation of NO release and induction of lipidperoxidation. Journal of Molecular Biochemistry **2013**;2:6-17
55. Kim JY, Park HD, Park E, Chon JW, et al. Growth-Inhibitory and Proapoptotic Effects of Alpha-Linolenic Acid on Estrogen-Positive Breast Cancer Cells. Annals of the New York Academy of Sciences **2009**;1171:190-5

Supplementary Information

Elution Gradient used for LC-MS

Buffer A composition:10 mM ammonium acetate in 95% acetonitrile, 5% water with 0.1% acetic acid
Buffer B composition: 10 mM ammonium acetate in 50% acetonitrile, 50% water with 0.1% acetic acid

Table S 1 *Corresponding elution gradient used for the chromatographic separation of metabolite extracts*

Retention (min)	Flow (mL/min)	%A	%B	Curve
0.000	0.500	99.0	1.0	5
1.000	0.500	99.0	1.0	5
3.000	0.500	85.0	15.0	5
6.000	0.500	50.0	50.0	5
9.000	0.500	5.0	95.0	5
10.000	0.500	5.0	95.0	5
10.500	0.500	99.0	1.0	5
14.000	0.500	99.0	1.0	5

LC-MS/MS method summary

- **Method Settings**

Application Mode: Small Molecule
Method duration (min): 14

- **Global Parameters**

Ion Source
- Ion Source type: H-ESI
- Spray Voltage: Static
- Positive Ion (V): 3900
- Negative Ion (V): 2700
- Gas Mode: Static
- Sheath Gas (Arb): 40
- Aux Gas (Arb): 10
- Sweep Gas (Arb): 1
- Ion Transfer Tube Temp (°C): 320
- Vaporizer Temp (°C): 300
- APPI Lamp: Not in use
- Use Ion Source settings from Tune: False
- FAIMS Mode: Not Installed

MS Global Settings
- Infusion Mode: Liquid Chromatography
- Expected LC Peak Width (s): 6
- Advanced Peak Determination: False
- Mild Trapping: True
- Default Charge State: 1
- Enable Xcalibur AcquireX method modifications: False
- Internal Mass Calibration: EASY-IC™
- Mode: Run Start

- **Experiment**

Start Time (min): 0
End Time (min): 14
Full Scan
- Orbitrap Resolution: 60,000
- Scan Range (m/z): 70-1050
- RF Lens (%): 50
- AGC Target: Standard
- Maximum Injection Time Mode: Custom
- Maximum Injection Time (ms): 100
- Microscans: 1
- Data Type: Profile
- Polarity: Positive/Negative
- Source Fragmentation: Disabled
- Use EASY-C™: On

- Filters

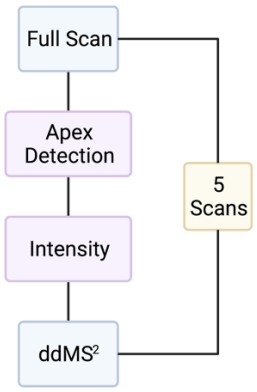

Apex Detection
Desired Apex Window (%): 50
Intensity
Intensity Threshold: 5.0e4
Data Dependent Mode: Number of Scans
Number of Dependent Scans: 5
ddMS^2 Scan
Multiplex Ions: False
Isolation Window (m/z): 2
Isolation Offset: Off
Collision Energy Type: Normalised
HCD Collision Energies (%): 15,30,45
Orbitrap Resolution: 15,000
Scan Range Mode: Auto
AGC Target: Standard
Maximum Injection Time Mode: Auto
Microscans: 1
Data Type: Profile
Use EASY-IC^{TM}: On

Mass Spectrometry Data Processing

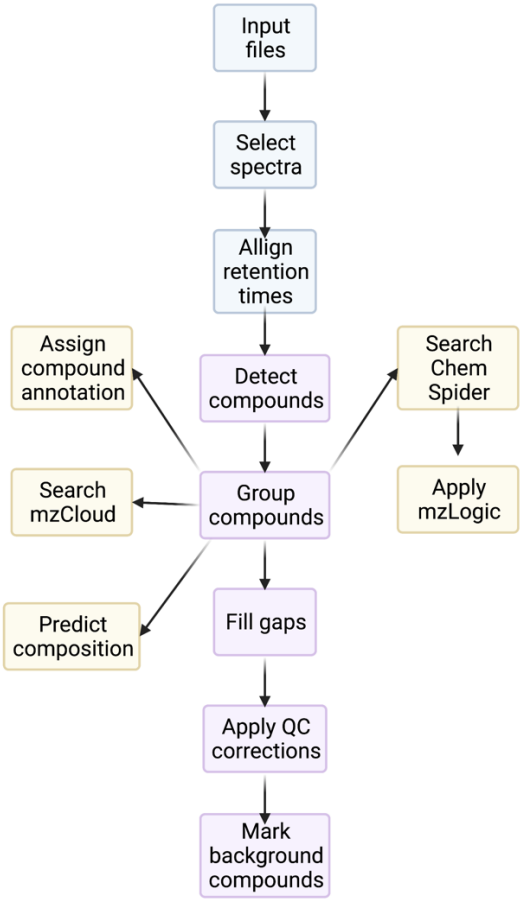

- **Input Files**

.raw data

- **Select Spectra**

Spectrum Properties Filter:
Lower RT Limit: 0
Upper RT Limit: 0
First Scan: 0
Last Scan: 0
Ignore Specified Scans: (not specified)
Lowest Charge State: 0
Highest Charge State: 0
Min. Precursor Mass: 0 Da
Max. Precursor Mass: 5000 Da
Total Intensity Threshold: 0
Minimum Peak Count: 1
Scan Event Filters:
Mass Analyzer: (not specified)
MS Order: Any
Activation Type: (not specified)
Min. Collision Energy: 0
Max. Collision Energy: 1000
Scan Type: Any
Polarity Mode: Is -
Peak Filters:
S/N Threshold (FT-only): 1.5

Replacements for Unrecognized Properties:
Unrecognized Charge Replacements: 1
Unrecognized Mass Analyzer Replacements: ITMS
Unrecognized MS Order Replacements: MS2
Unrecognized Activation Type Replacements: CID
Unrecognized Polarity Replacements: +
Unrecognized MS Resolution@200 Replacements: 60000
Unrecognized MSn Resolution@200 Replacements: 30000
General Settings:
Precursor Selection: Use MS(n - 1) Precursor
Use Isotope Pattern in Precursor Reevaluation: True
Provide Profile Spectra: Automatic
Store Chromatograms: False

- Align Retention Times

General Settings:
Alignment Model: Adaptive curve
Alignment Fallback: None
Maximum Shift [min]: 0.3
Shift Reference File: True
Mass Tolerance: 3 ppm
Remove Outlier: True

- Detect Compounds

General Settings:
Mass Tolerance [ppm]: 3 ppm
Intensity Tolerance [%]: 30
S/N Threshold: 3
Min. Peak Intensity: 500000
Base Ions: [M+H]+1; [M-H]-1
Min. Element Counts: C H
Max. Element Counts: C90 H190 Br3 Cl4 K2 N10 Na2 O15 P6 S5
Peak Detection:
Filter Peaks: True
Max. Peak Width [min]: 0.5
Remove Singlets: True
Min. # Scans per Peak: 5
Min. # Isotopes: 1
Isotope Grouping:
Min. Spectral Distance Score: 0
Remove Potentially False Positive Isotopes: True

- Group Compounds

Compound Consolidation:
Mass Tolerance: 5 ppm
RT Tolerance [min]: 0.2
Fragment Data Selection:
Preferred Ions: [M+H]+1; [M-H]-1

- Fill Gaps

General Settings:
Mass Tolerance: 5 ppm
S/N Threshold: 1.5
Use Real Peak Detection: True

- Apply QC Correction

General Settings:
Regression Model: Linear
Min. QC Coverage [%]: 30
Max. QC Area RSD [%]: 30
Max. Corrected QC Area RSD [%]: 25
Max. # Files Between QC Files: 15

- Mark Background Compounds

General Settings:
Max. Sample/Blank: 5
Max. Blank/Sample: 0
Hide Background: True

- Search ChemSpider

Search Settings:
Database(s): ChEBI; Human Metabolome Database
Search Mode: By Formula or Mass
Mass Tolerance: 5 ppm
Max. # of results per compound: 100
Max. # of Predicted Compositions to be searched per Compound: 3
Result Order (for Max. # of results per compound): Order By Reference Count (DESC)
Predicted Composition Annotation:
Check All Predicted Compositions: False

- Apply mzLogic

Search Settings:
FT Fragment Mass Tolerance: 10 ppm
IT Fragment Mass Tolerance: 0.4 Da
Max. # Compounds: 0
Max. # mzCloud Similarity Results to consider per Compound: 10
Match Factor Threshold: 30

- Predict Compositions

Prediction Settings:
Mass Tolerance: 5 ppm
Min. Element Counts: C H
Max. Element Counts: C90 H190 Br3 Cl4 N10 O18 P3 S5
Min. RDBE: 0
Max. RDBE: 40
Min. H/C: 0.1
Max. H/C: 4
Max. # Candidates: 10
Max. # Internal Candidates: 200
Pattern Matching:
Intensity Tolerance [%]: 30
Intensity Threshold [%]: 0.1
S/N Threshold: 3
Min. Spectral Fit [%]: 30
Min. Pattern Cov. [%]: 90
Use Dynamic Recalibration: True
Fragments Matching:
Use Fragments Matching: True

Mass Tolerance: 5 ppm
S/N Threshold: 3

- Assign Compound Annotations

General Settings:
Mass Tolerance: 5 ppm
Data Sources:
Data Source #1: mzCloud Search
Data Source #2: Predicted Compositions
Data Source #3: MassList Search
Data Source #4: ChemSpider Search
Data Source #5: Metabolika Search
Data Source #6: (not specified)
Data Source #7: (not specified)
Scoring Rules:
Use mzLogic: True
Use Spectral Distance: True
SFit Threshold: 20
SFit Range: 20

- Search mzCloud

General Settings:
Compound Classes: All
Precursor Mass Tolerance: 10 ppm
FT Fragment Mass Tolerance: 10 ppm
IT Fragment Mass Tolerance: 0.4 Da
Library: Autoprocessed; Reference
Post Processing: Recalibrated
Max. # Results: 10
Annotate Matching Fragments: True
DDA Search:
Identity Search: Cosine
Match Activation Type: True
Match Activation Energy: Match with Tolerance
Activation Energy Tolerance: 20
Apply Intensity Threshold: True
Similarity Search: None
Match Factor Threshold: 60
DIA Search:
Use DIA Scans for Search: False
Max. Isolation Width [Da]: 500
Match Activation Type: False
Match Activation Energy: Any
Activation Energy Tolerance: 100
Apply Intensity Threshold: False
Match Factor Threshold: 20

- Differential Analysis

General Settings:
Log10 Transform Values: True

ANOVA analysis of olaparib dose-dependent DNA DSB immunofoci formation

Table S 2 Corresponding p-values obtained from single-factor ANOVA analysis of dose-dependent γH2AX and 53BP1 foci formation following seven day exposure to olaparib in MCF-7, MDA-MB-231 and HCC1937 cells

Cell line	Foci	p-value
MCF-7	*53BP1*	0.011
	γH2AX	4.876×10^{-10}
MDA-MB-231	*53BP1*	0.0009
	γH2AX	4.096×10^{-10}
HCC1937	*53BP1*	1.204×10^{-6}
	γH2AX	1.441×10^{-5}

Panel of individual PCA pairwise analysis of MCF7, MDA-MB-231 and HCC1937 at their relative IC_{10}, IC_{25} and IC_{50} doses of Olaparib

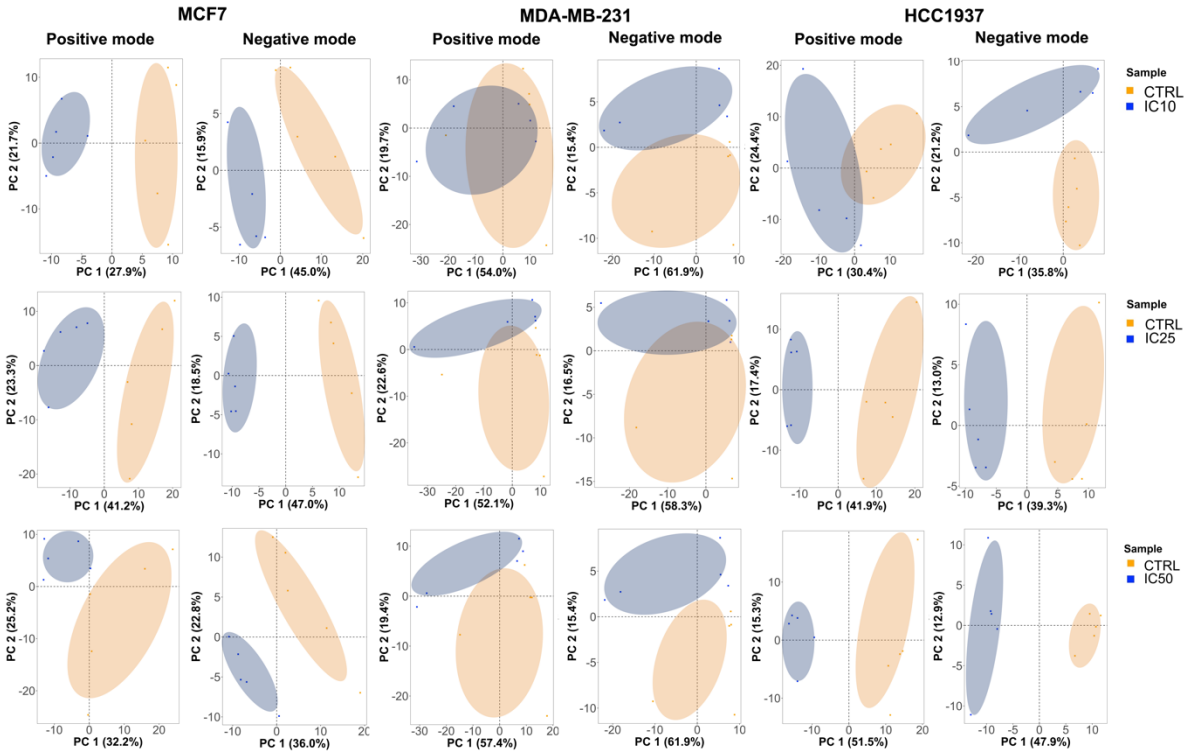

Figure S 1 PCA pairwise analysis of untargeted metabolomics data collected, in both positive and negative mode, from MCF7, MDA-MB-231, and HCC1937 cells treated with their relative IC_{10}, IC_{25} and IC_{50} doses of Olaparib. For each sample, 5 replicate were used. Data points in

the two dimensional PCA score plot were central scaled. The plot was designed on R through the ggplot2 graphical package

Pairwise differential analysis of metabolites identified in MCF7, MDA-MB-231 and HCC1937 cells in positive and negative mode

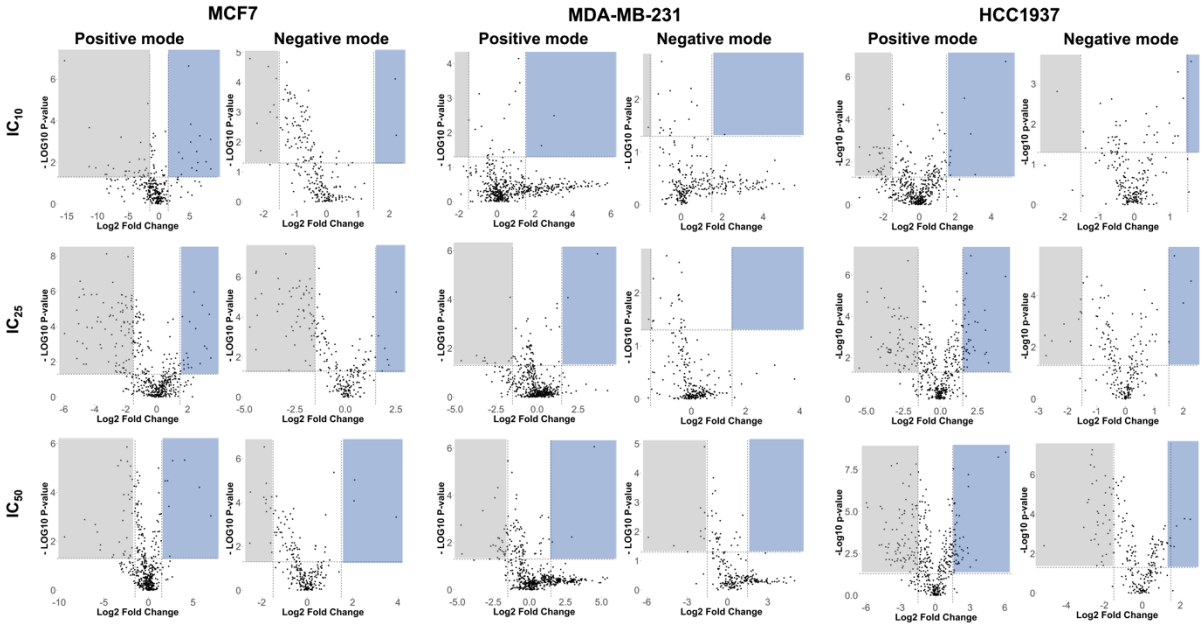

Figure S 2 Volcano plots show the log2 fold change and the -log10 adjusted p-values in metabolite levels induced by treatment with different doses of Olaparib (IC_{10}, IC_{25}, and IC_{50}) in MCF7, MDA-MB-231 and HCC1937 cells. Data were selected at the cut off values adj-p<0.05 and fold change >1.5. Blue and grey boxes indicate metabolites having their levels significantly upregulated and downregulated in the different samples, respectively.

Table S 2 Global differential metabolites between samples treated with IC_{10}, IC25 and IC_{50} of Olaparib and their relative control (non-treated) samples. Metabolites identified in both positive and negative mode with p-value = <0.05 and Log2 Fold Change = >1.5.

Sample	HESI +	HESI -
MCF7 IC10/Ctrl	41	10
MCF7 IC25/Ctrl	111	62
MCF7 IC50/Ctrl	41	15
MDA231 IC10/Ctrl	2	1
MDA231 IC25/Ctrl	12	1
MDA231 IC50/Ctrl	34	9
HCC1937 IC10/Ctrl	36	2
HCC1937 IC25/Ctrl	107	13
HCC1937 IC50/Ctrl	134	43

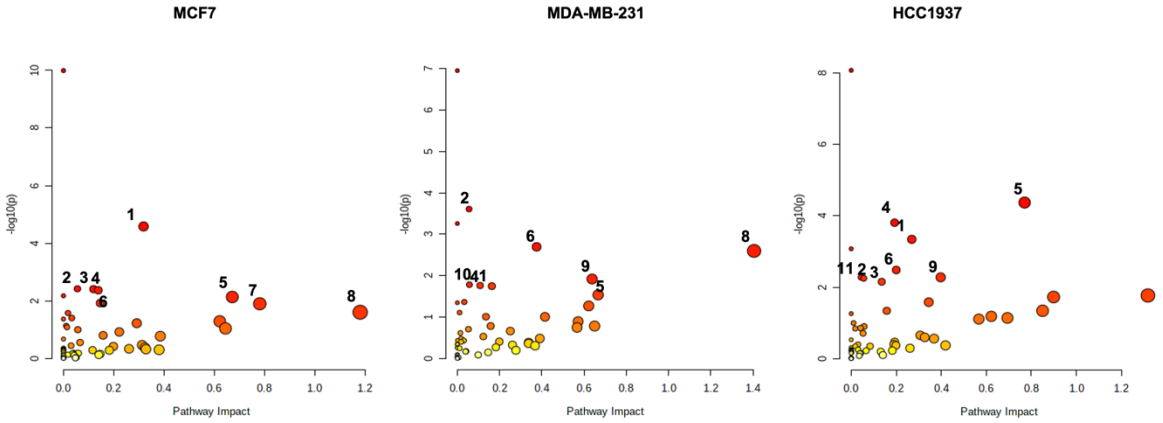

1. Alanine, aspartate and glutamate metabolism
2. Glutamine and glutamate metabolism
3. Histidine metabolism
4. Arginine and proline metabolism
5. Glycine, serine and threonine metabolism
6. Arginine biosynthesis
7. Sphingolipid metabolism
8. Glycerophospholipid metabolism
9. Glutathione metabolism
10. Taurine and hypotaurine metabolism
11. Glyoxylate and dicarboxylate metabolism

Figure S 3 Enrichment analysis of non-treated MCF7, MDA-MB-231 and HCC1937 cells.

Table S 3 Enriched metabolic pathways in different breast cancer cells (MCF7, MDA-MB-231, and HCC1937) before and after treatment with IC_{50} dose of Olaparib. FDR = False Discovery Rate.

- Olaparib

MCF7

Pathways	P-value	FDR	Impact
Aminoacyl-tRNA biosynthesis	1.02E-10	8.57E-09	0
Alanine, aspartate and glutamate metabolism	2.63E-05	0.001104	0.31879
Glutamine and glutamate metabolism	3.83E-03	0.072247	0.055556
Histidine metabolism	3.94E-03	0.072247	0.11935
Arginine and proline metabolism	4.30E-03	0.072247	0.13859
Valine, leucine and isoleucine biosynthesis	0.006688	0.088594	0
Glycine, serine and threonine metabolism	0.007382	0.088594	0.67221
Arginine biosynthesis	0.012025	0.11847	0.14615
Sphingolipid metabolism	0.012694	0.11847	0.78164
Glycerophospholipid metabolism	0.025021	0.20274	1.1815

MDA-MB-231

Pathways	P-value	FDR	Impact
Aminoacyl-tRNA biosynthesis	1.11E-07	9.31E-06	0
Glutamine and glutamate metabolism	0.000246	0.010315	0.055556
Valine, leucine and isoleucine biosynthesis	0.000549	0.015362	0
Arginine biosynthesis	0.00201	0.042201	0.37538
Glycerophospholipid metabolism	0.002519	0.042319	1.4051
Glutathione metabolism	0.012023	0.16708	0.63816
Taurine and hypotaurine metabolism	0.016455	0.16708	0.057143
Arginine and proline metabolism	0.017286	0.16708	0.10783
Alanine, aspartate and glutamate metabolism	0.017902	0.16708	0.16342
Glycine, serine and threonine metabolism	0.029087	0.24434	0.66667

HCC1937

Pathways	P-value	FDR	Impact
Aminoacyl-tRNA biosynthesis	8.36E-09	7.03E-07	0
Glycine, serine and threonine metabolism	4.24E-05	0.001781	0.77013
Arginine and proline metabolism	0.000156	0.004357	0.19275
Alanine, aspartate and glutamate metabolism	0.000455	0.009555	0.26907
Valine, leucine and isoleucine biosynthesis	0.00084	0.014109	0
Arginine biosynthesis	0.003289	0.046045	0.2
Glyoxylate and dicarboxylate metabolism	0.005277	0.052485	0.043771
Glutathione metabolism	0.005277	0.052485	0.39739
Glutamine and glutamate metabolism	0.005623	0.052485	0.055556
Histidine metabolism	0.007034	0.05908	0.13548

+ Olaparib

Pathways	P-value	FDR	Impact
Aminoacyl-tRNA biosynthesis	8.19E-10	6.88E-08	0
Arginine biosynthesis	4.37E-06	0.000184	0.54769
Alanine, aspartate and glutamate metabolism	1.31E-05	0.000366	0.25749
Arginine and proline metabolism	0.000141	0.002965	0.20848
Glutamine and glutamate metabolism	0.000363	0.006102	0.055556
Valine, leucine and isoleucine biosynthesis	0.000807	0.011293	0
Taurine and hypotaurine metabolism	0.002633	0.0316	0.085714
Glycine, serine and threonine metabolism	0.003952	0.040556	0.67221
Butanoate metabolism	0.004345	0.040556	0.12169
Vitamin B6 metabolism	0.00747	0.062741	0.96579

Pathways	P-value	FDR	Impact
Aminoacyl-tRNA biosynthesis	4.87E-08	4.09E-06	0
Arginine biosynthesis	4.44E-05	0.001297	0.54769
Valine, leucine and isoleucine biosynthesis	4.63E-05	0.001297	0
Glutamine and glutamate metabolism	0.000348	0.007318	0.055556
Arginine and proline metabolism	0.002382	0.040027	0.19139
Glycine, serine and threonine metabolism	0.003697	0.05176	0.35674
Alanine, aspartate and glutamate metabolism	0.007553	0.087816	0.25155
Pantothenate and CoA biosynthesis	0.008364	0.087816	0.025568
Cysteine and methionine metabolism	0.016897	0.1577	0.74161
Taurine and hypotaurine metabolism	0.020936	0.17277	0.057143

Pathways	P-value	FDR	Impact
Aminoacyl-tRNA biosynthesis	6.05E-09	5.08E-07	0
Arginine biosynthesis	4.03E-06	0.000169	0.54769
Alanine, aspartate and glutamate metabolism	7.18E-05	0.002011	0.25692
Glutamine and glutamate metabolism	0.000348	0.007318	0.055556
Arginine and proline metabolism	0.000585	0.009829	0.19275
Valine, leucine and isoleucine biosynthesis	0.000774	0.010591	0
Glycine, serine and threonine metabolism	0.000883	0.010591	0.37754
Taurine and hypotaurine metabolism	0.002532	0.02658	0.085714
Cysteine and methionine metabolism	0.004844	0.045211	0.67619
Butanoate metabolism	0.022626	0.19004	0.12169

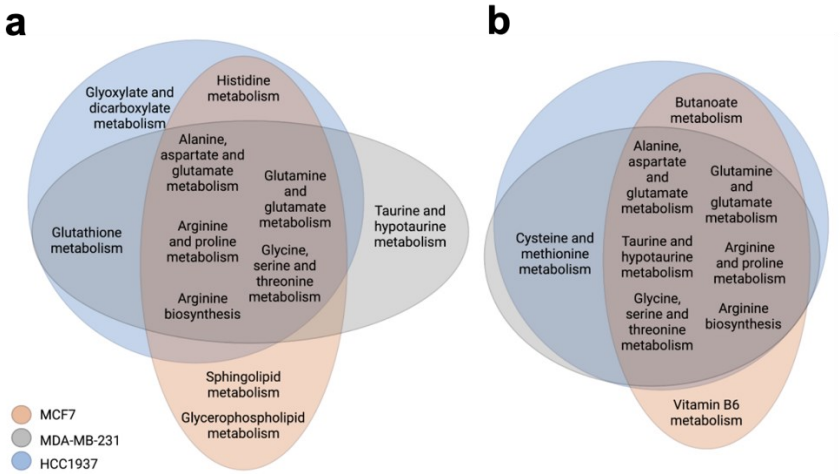

Figure S 4 *Venn diagram representing the enriched metabolic pathways in MCF7, MDA-MB-231 and HCC1937 cells.a) Metabolic pathways in the absence of the drug and b) following seven days treatment with olaparib at* IC_{50} *doses.*

Table S 4 Classification of the relevant metabolites identified in MCF7, MDA-MB-231 and HCC1937 at all Olaparib doses (IC_{10}, IC_{25} and IC_{50}) after seven days treatment. The table shows the class, name, Log_2 fold change, and the p-value (p) of each compound. PC: phosphocholine; PE: phosphoethanolamine; PUFA: poly unsaturated fatty acid; SM: Sfingomyelin.

		MCF7						MDA-MB-231						HCC1937					
Class	**Name**	**Log_2 fold change IC10**	***p***	**Log_2 fold change IC25**	***p***	**Log_2 fold change IC50**	***p***	**Log_2 fold change IC10**	***p***	**Log_2 fold change IC25**	***p***	**Log_2 fold change IC50**	***p***	**Log_2 fold change IC10**	***p***	**Log_2 fold change IC25**	***p***	**Log_2 fold change IC50**	***p***
Amide	**Nicotinamide**	-0.54	*0.08*	-0.54	*0.26*	-0.14	*0.29*	-0.07	*0.50*	-0.16	*0.05*	-0.45	*0.03*	0.35	0.07	0.33	0.01	-0.1	0.28
Amine	**N-Oleoyl ethanolamine**	-1.48	*0.13*	-0.81	*0.63*	-0.08	*0.61*	-0.46	*0.29*	-3.19	*0.02*	-0.61	*0.26*	-1.64	0.17	-2.48	0.03	-1.16	0.02
Amine	**Triethanolamine**	1.03	*0.56*	-0.6	*0.03*	0.05	*0.15*	2.87	*0.43*	0.57	*0.76*	3.05	*0.41*	-0.46	0.47	0.42	0.13	0.39	0.50
Amino acid	**3-Sulfinoalanine**	-1.05	*0.45*	-1.75	*0.03*	-1.07	*0.15*	-	-	-0.65	*0.33*	-	-	0.32	0.71	-0.41	0.64	-0.67	0.02
Amino acid	**4-Guanidinobutanoic acid**	-1.26	*0.01*	-2.03	*0.00*	-1.13	*0.00*	-0.22	*0.49*	-0.28	*0.57*	-0.46	*0.16*	-1.03	0.08	-1.82	0.01	-1.81	0.00
Amino acid	**4-Hydroxyproline**	-1.01	*0.00*	-2.1	*0.00*	-1.08	*0.01*	-0.37	*0.16*	-	-	-0.39	*0.14*	-0.33	0.44	-0.3	0.33	-0.87	0.02
Amino acid	**4-Oxoproline**	-0.7	*0.34*	0.88	*0.03*	0.16	*0.24*	0.36	*0.55*	-0.27	*0.03*	0.81	*0.06*	0.64	0.03	1.03	0.01	1.47	0.00
Amino acid	**Betaine**	-	-	-0.84	*0.00*	-0.04	*0.72*	-0.02	*0.26*	-0.17	*0.11*	-0.44	*0.02*	-0.05	0.72	-0.03	0.49	-0.39	0.00
Amino acid	**Choline**	-3.71	*0.11*	-2.14	*0.02*	-2.11	*0.07*	0.06	*0.46*	-1.3	*0.03*	-1.53	*0.00*	-2.08	0.00	-2.87	0.00	-3.71	0.00
Amino acid	**Citrulline**	-0.27	*0.58*	1.76	*0.01*	-0.39	*0.04*	-0.33	*0.22*	-0.25	*0.05*	-0.29	*0.02*	-0.08	0.47	0.31	0.51	0.06	0.91
Amino acid	**Creatine**	-0.31	*0.57*	-1.68	*0.00*	-0.47	*0.05*	-0.82	*0.01*	-0.35	*0.18*	-1.12	*0.01*	0.05	0.26	-0.37	0.03	-0.7	0.01
Amino acid	**Creatinine**	-	-	-0.12	*0.18*	0.1	*0.73*	-0.46	*0.04*	-0.38	*0.06*	-0.36	*0.15*	-0.13	0.44	0.31	0.37	-0.2	0.28
Amino acid	**Gamma-Aminobutyric acid**	-0.93	*0.00*	-1.75	*0.00*	-0.74	*0.00*	-0.16	*0.14*	-0.09	*0.15*	-0.2	*0.14*	-0.21	0.71	0.02	0.87	-0.52	0.00
Amino acid	**Glycine**	-1.26	*0.00*	-2.08	*0.00*	-0.99	*0.00*	-	-	-	-	-	-	-	-	-	-	-	-
Amino acid	**Hypotaurine**	0.29	*0.30*	-0.35	*0.10*	-0.61	*0.03*	0.25	*0.55*	-0.2	*0.07*	-0.54	*0.00*	-0.72	0.02	-0.55	0.00	-1.26	0.00
Amino acid	**L-Alanine**	-0.83	*0.00*	-1.66	*0.00*	-0.91	*0.01*	-	-	-	-	-	-	-	-	-	-	-	-

Amino acid	**L-Arginine**	6.65	*0.00*	-0.46	*0.02*	-0.07	*0.56*	-0.08	*0.56*	-0.14	*0.65*	0.25	*0.36*	0.02	0.49	0.25	0.06	-0.19	0.08
Amino acid	**L-Asparagine**	0.3	*0.33*	-0.38	*0.22*	0.99	*0.04*	-	-	-	-	-	-	0.9	0.16	1.07	0.13	1.31	0.13
Amino acid	**L-Aspartic acid**	-0.64	*0.04*	-2.2	*0.00*	-1.38	*0.00*	0.32	*0.07*	0.33	*0.27*	0.79	*0.02*	-0.14	0.89	-0.5	0.01	-1.62	0.00
Amino acid	**L-Cystathionine**	5.15	*0.00*	-2.06	*0.00*	-0.32	*0.12*	-0.13	*0.93*	1.19	*0.42*	0.79	*0.64*	-1.68	0.00	-2.2	0.00	-3.8	0.00
Amino acid	**L-Glutamic acid**	-1.26	*0.00*	-2.08	*0.00*	-1.3	*0.00*	-0.35	*0.53*	-0.71	*0.02*	-1.14	*0.00*	-0.4	0.11	-0.49	0.03	-2.06	0.00
Amino acid	**L-Glutamine**	-11.37	*0.02*	-0.97	*0.00*	-0.38	*0.06*	-0.05	*0.20*	0.17	*0.43*	-0.09	*0.71*	-0.21	0.03	-0.32	0.00	-0.51	0.00
Amino acid	**L-Isoleucine**	-	-	-1.49	*0.27*	-0.59	*0.97*	-1.39	*0.98*	1.52	*0.31*	-0.28	*0.65*	0.07	0.18	-0.56	0.73	0.12	0.95
Amino acid	**L-Leucine**	-	-	-1.39	*0.00*	-0.41	*0.12*	0.22	*0.40*	-	-	-0.5	*0.07*	-	-	-0.63	0.04	-1.31	0.00
Amino acid	**L-Lysine**	-1.11	*0.01*	-1.04	*0.02*	-0.42	*0.34*	-0.3	*0.07*	-0.41	*0.12*	0.09	*0.47*	0.18	0.25	0.28	0.01	-0.35	0.00
Amino acid	**L-Methionine**	-0.93	*0.00*	-2.25	*0.00*	-1.04	*0.00*	-0.07	*0.23*	-0.31	*0.03*	-0.39	*0.11*	0.06	0.96	-0.14	0.23	-0.87	0.00
Amino acid	**L-Ornithine**	-	-	-	-	-	-	-	-	-	-	-	-	0.18	0.55	0.29	0.08	-0.12	0.66
Amino acid	**L-Phenylalanine**	-1.31	*0.74*	-	-	-	-	-0.12	*0.36*	-0.37	*0.03*	-0.28	*0.05*	-0.18	0.86	-0.32	0.19	-0.72	0.00
Amino acid	**L-Proline**	-1.26	*0.00*	2.04	*0.12*	-0.33	*0.53*	0.07	*0.64*	-0.25	*0.44*	-0.39	*0.14*	-	-	-	-	-	-
Amino acid	**L-Serine**	2.18	*0.00*	2.52	*0.00*	2.09	*0.00*	0.25	*0.23*	0.33	*0.45*	0.88	*0.00*	-0.09	0.69	-0.33	0.01	-0.97	0.00
Amino acid	**L-Tryptophan**	-1.57	*0.00*	-2.36	*0.00*	-1.34	*0.00*	-0.33	*0.07*	-0.77	*0.03*	-0.91	*0.01*	-0.27	0.48	-0.75	0.02	-0.84	0.00
Amino acid	**L-Tyrosine**	0.08	*0.71*	-2.29	*0.00*	-1.25	*0.00*	-0.35	*0.03*	-0.51	*0.00*	-0.55	*0.02*	0.11	0.02	-0.36	0.13	-1	0.01
Amino acid	**L-Valine**	-1.16	*0.00*	-1.41	*0.00*	-0.56	*0.01*	0.12	*0.58*	0.09	*0.91*	0.36	*0.96*	0.07	0.84	0.21	0.97	0.58	0.40
Amino acid	**N-a-Acetyl-L-arginine**	-	-	-1.61	*0.00*	-0.64	*0.01*	0.49	*0.52*	-0.19	*0.36*	-0.55	*0.13*	-0.34	0.22	0	0.50	-0.39	0.02
Amino acid	**N-Acetylaspartyl glutamic acid**	-0.53	*0.11*	-1.53	*0.00*	-0.68	*0.07*	0.2	*0.68*	-0.27	*0.39*	-0.06	*0.19*	-1.29	0.01	-0.83	0.00	-2.86	0.00
Amino acid	**N-Acetylisoleucine**	-0.13	*0.02*	0.25	*0.09*	-0.05	*0.52*	2.42	*0.36*	0.37	*0.77*	1.37	*0.49*	0.02	0.64	0.13	0.02	0.11	0.20
Amino acid	**N-Acetylleucine**	-	-	0.87	*0.65*	0.44	*0.74*	-	-	0.43	*0.59*	-	-	-	-	-	-	0.7	0.45
Amino acid	**N-Acetyltaurine**	-0.37	*0.05*	-0.82	*0.00*	-0.65	*0.01*	0.14	*0.91*	-0.16	*0.22*	-5.89	*0.02*	-0.74	0.13	-0.7	0.01	-1.08	0.00
Amino acid	**Ornithine**	4.83	*0.00*	-0.4	*0.25*	-0.23	*0.22*	-0.54	*0.08*	-0.61	*0.01*	-0.26	*0.19*	0.18	0.55	0.29	0.08	-0.12	0.66

Amino acid	**Pyroglutamic acid**	-10.3	*0.02*	-0.73	*0.03*	-0.17	*0.51*	-0.05	*0.20*	0.19	*0.42*	-0.29	*0.56*	-0.25	0.01	-0.34	0.01	-0.61	0.00
Amino acid	**Taurine**	-0.37	*0.05*	-0.82	*0.00*	-0.65	*0.01*	0.14	*0.91*	-0.16	*0.22*	-5.89	*0.02*	-0.74	0.13	-0.7	0.01	-1.08	0.00
Amino acid	**Thiamine**	5.36	*0.38*	-1.22	*0.00*	-0.87	*0.00*	-1.15	*0.01*	-0.44	*0.05*	-0.31	*0.25*	-0.3	0.47	-0.15	0.43	-1.07	0.00
Amino acid	**Threonine**	0.06	*0.36*	1.4	*0.50*	0.57	*0.94*	-1.9	*0.60*	-0.52	*0.09*	0.64	*0.51*	-0.22	0.66	-0.3	0.08	0.67	0.34
Benzenoid	**Benzoic acid**	0.64	*0.86*	0.3	*0.43*	0.11	*0.43*	0.39	*0.02*	0.13	*0.56*	0.34	*0.39*	-0.17	0.25	-0.24	0.04	0.76	0.01
Carbohydrate	**D-Glucose**	-0.23	*0.94*	0.96	*0.02*	0.21	*0.23*	-0.21	*0.38*	-0.37	*0.04*	0.09	*0.17*	1.09	0.03	0.92	0.00	0.84	0.00
Carbohydrate	**Glyceraldehyde 3-phosphate**	-1.45	*0.00*	-2.31	*0.00*	-1.43	*0.00*	0.22	*0.27*	-0.22	*0.18*	-1.31	*0.02*	0.19	0.86	-0.26	0.28	-1.7	0.00
Carbohydrate	**Mannose 6-phosphate**	-0.32	*0.20*	-0.72	*0.09*	-0.2	*0.30*	0.78	*0.01*	0.01	*0.87*	0.22	*0.31*	0.33	0.01	0.67	0.00	0.47	0.02
Carbohydrate	**N-Acetyl-glucosamine 1-phosphate**	-1.31	*0.00*	-2.41	*0.00*	-1.56	*0.00*	-0.14	*0.09*	-0.63	*0.00*	-1.21	*0.00*	-	-	-	-	-	-
Carbohydrate	**Threonic acid**	-0.73	*0.03*	-0.91	*0.01*	-0.3	*0.68*	-0.53	*0.04*	-0.33	*0.11*	-0.78	*0.02*	-0.51	0.01	-0.59	0.00	-1.62	0.00
Carboxylic acid	**5-L-Glutamyl-taurine**	2.22	*0.01*	1.24	*0.01*	2.07	*0.00*	-	-	-	-	-	-	-	-	-	-	-	-
Carboxylic acid	**Citric acid**	-0.43	*0.08*	-1.27	*0.00*	-0.3	*0.20*	0.1	*0.81*	-0.23	*0.94*	-	-	-	-	-	-	-0.91	0.00
Carboxylic acid	**Dodecanedioic acid**	0.42	*0.70*	0.65	*0.06*	0.47	*0.09*	1.82	*0.40*	0.07	*0.66*	-1.08	*0.63*	0.25	0.33	0.28	0.15	0.43	0.11
Carboxylic acid	**Fumaric acid**	-	-	-	-	-	-	-	-	-	-	-	-	0.3	0.16	0.11	0.09	-2.33	0.00
Carboxylic acid	**L-Lactic acid**	-0.58	*0.02*	-0.45	*0.07*	0.41	*0.26*	0.05	*0.65*	-0.37	*0.04*	-0.46	*0.09*	-0.08	0.84	0.1	0.27	-0.93	0.00
Carboxylic acid	**Phthalic acid**	-	-	-1.55	*0.00*	-0.68	*0.47*	-0.52	*0.65*	0.66	*0.34*	-	-	-	-	-	-	-	-
Carboxylic acid	**Pyruvic acid**	-0.69	*0.01*	-0.99	*0.00*	-0.64	*0.00*	1.74	*0.45*	-0.33	*0.95*	-0.01	*0.10*	-0.51	0.01	-0.61	0.00	-1.22	0.00
Carboxylic acid	**Succinic acid**	-0.87	*0.11*	-1.21	*0.05*	-0.64	*0.25*	-	-	-	-	-	-	-	-	-	-	-	-

Carboxylic acid	**Tetradecanedioic acid**	-0.36	*0.10*	-0.22	*0.28*	-0.56	*0.04*	-	-	-	-	-	-	0.17	0.43	0.12	0.53	0.21	0.11
Carnitine	**2-Methylbutyroyl carnitine**	-0.71	*0.00*	-1.99	*0.00*	-1.15	*0.00*	0.06	*0.98*	-0.36	*0.02*	-0.9	*0.00*	-0.3	0.10	-1.16	0.00	-3.31	0.00
Carnitine	**Butenylcarnitine**	-	-	1.09	*0.29*	-0.16	*0.60*	1.2	*0.00*	1.88	*0.00*	2.94	*0.01*	1.11	0.30	1.5	0.00	1.19	0.01
Carnitine	**Decanoylcarnitine**	0.41	*0.81*	-0.09	*0.97*	0.22	*0.97*	0.04	*0.90*	-1.42	*0.31*	1.01	*0.89*	-1.45	0.60	-0.9	0.59	-0.71	0.96
Carnitine	**Dodecanedioyl carnitine**	-1.31	*0.38*	0.61	*0.11*	0.01	*0.95*	2.94	*0.47*	0.86	*0.59*	-	-	1.22	0.02	1.13	0.04	1.77	0.00
Carnitine	**Heptadecanoyl carnitine**	-	-	-1.82	*0.37*	1.25	*0.00*	0.24	*0.72*	-0.97	*0.06*	-0.38	*0.33*	0.67	0.68	0.24	0.84	1.2	0.04
Carnitine	**L-Carnitine**	-0.17	*0.82*	0.03	*0.54*	-0.35	*0.11*	-0.38	*0.40*	0.39	*0.79*	1.69	*0.58*	1.07	0.05	0.53	0.07	0.98	0.00
Carnitine	**L-Hexanoylcarnitine**	0.56	*0.55*	1.38	*0.27*	-0.03	*1.00*	-0.37	*0.12*	-1.3	*0.00*	-1.62	*0.00*	-0.88	0.00	1.75	0.00	1.71	0.00
Carnitine	**L-Palmitoylcarnitine**	-8.48	*0.19*	0.34	*0.53*	0.47	*0.49*	0.13	*0.86*	-0.89	*0.13*	-0.92	*0.11*	0.05	0.69	1.24	0.09	1.63	0.03
Carnitine	**Pentadecanoyl carnitine**	-1.63	*0.15*	-0.49	*0.14*	0.03	*0.92*	0.72	*0.21*	-	-	-1.17	*0.84*	-1.05	0.09	-2.71	0.00	-1.37	0.02
Carnitine	**Propionylcarnitine**	-15.38	*0.00*	-1.42	*0.21*	-0.65	*0.63*	0.12	*0.85*	0.17	*0.86*	-0.87	*0.00*	0.14	0.61	-0.89	0.02	-2.79	0.00
Carnitine	**Stearoylcarnitine**	-1.15	*0.85*	2.03	*0.01*	2.42	*0.06*	-0.37	*0.91*	-1.02	*0.17*	-0.68	*0.21*	1.09	0.21	1.6	0.03	2.06	0.01
Carnitine	**Tiglylcarnitine**	-0.41	*0.11*	-0.29	*0.02*	0.22	*0.40*	0.04	*0.87*	-0.15	*0.07*	-0.46	*0.04*	0.05	0.30	0.09	0.31	-1.88	0.00
Carnitine	**trans-2-Dodecenoylcarnitine**	-0.98	*0.55*	0.81	*0.78*	-0.53	*0.18*	-0.57	*0.78*	-0.35	*0.07*	0.32	*0.33*	-0.88	0.02	-0.53	0.07	-0.82	0.00
Carnitine	**trans-Hexadec-2-enoyl carnitine**	-	-	-0.74	*0.05*	0.39	*0.93*	0.2	*0.75*	-0.91	*0.19*	-0.51	*0.29*	-0.76	0.11	-1.24	0.01	-1.18	0.01
Ceramide	**Cer(d18:1/16:0)**	-0.62	*0.22*	-2.41	*0.02*	-0.66	*0.09*	0.42	*0.93*	-1.65	*0.11*	-1.28	*0.15*	-1.47	0.02	-	-	-2.71	0.00
Ceramide	**Cer(d18:1/24:1(15Z))**	-2.34	*0.14*	-2.65	*0.02*	-3.01	*0.07*	-	-	-	-	-	-	-1.52	0.12	-3.55	0.01	-3.72	0.01
Cholesterol ester	**Cholesteryl acetate**	-1.41	*0.62*	-0.91	*0.04*	-0.8	*0.18*	-0.09	*0.16*	-0.4	*0.10*	-1.31	*0.00*	-	-	-	-	-	-
Fatty acid	**Glycerol 3-phosphate**	-1	*0.00*	-1.57	*0.00*	-0.66	*0.01*	-0.56	*0.11*	-0.79	*0.14*	-2	*0.00*	-0.11	0.61	0.02	0.93	-0.77	0.02
Fatty acid	**Linoleamide**	-2.79	*0.12*	-1.52	*0.63*	-0.07	*0.97*	-0.06	*0.56*	-3.04	*0.04*	0.04	*0.68*	-1.17	0.38	-0.8	0.36	-1.23	0.29
Fatty acid	**Stearic acid**	-0.4	*0.47*	0.43	*0.44*	-0.27	*0.59*	0.24	*0.76*	0.72	*0.80*	0.74	*0.72*	0.25	0.45	0.31	0.10	0.74	0.00

Fatty acid	**Stearoylethanolamide**	-	-	-	-	-	-	-	-	-1.21	*0.03*	-1.25	*0.03*	-0.78	0.59	-1.33	0.17	-1.38	0.13
Fatty acid	**Tetraglyme**	-	-	0.72	*0.11*	-2.02	*0.04*	0.82	*0.39*	0.68	*0.82*	2.35	*0.18*	0.73	0.08	0.38	0.01	0.89	0.00
Fatty amide	**Oleamide**	-2.79	*0.12*	-1.52	*0.63*	-0.07	*0.97*	-0.06	*0.56*	-3.04	*0.04*	0.04	*0.68*	-1.17	0.38	-0.8	0.36	-1.23	0.29
Furanone	**Ascorbic acid**	-0.03	*0.96*	-0.83	*0.03*	-0.21	*0.24*	1.34	*0.49*	-	-	1.43	*0.34*	-2.16	0.00	-1.55	0.00	-0.25	0.09
Inorganic compound	**Pyrophosphate**	-0.04	*0.29*	0.93	*0.01*	0.48	*0.19*	0.55	*0.31*	0.63	*0.15*	0.94	*0.02*	0.88	0.07	1.51	0.01	1.67	0.00
Keto acid	**Acetoacetic acid**	7.66	*0.01*	-0.48	*0.00*	-0.04	*0.23*	-0.07	*0.39*	-0.21	*0.05*	-0.69	*0.00*	-0.17	0.34	-0.42	0.02	-1.47	0.00
Keto acid	**alpha-Ketoglutaric acid**	-0.39	*0.01*	-1.35	*0.00*	0.35	*0.01*	0.49	*0.01*	0.12	*0.20*	-0.3	*0.13*	-0.64	0.00	-0.35	0.04	-0.62	0.01
Keto acid	**Levulinic acid**	-	-	-	-	-	-	-	-	-1.14	*0.01*	-0.57	*0.03*	-1.08	0.09	-0.77	0.01	-2.36	0.00
Nucleobase	**Adenine**	-1.24	*0.00*	-1.92	*0.00*	-0.76	*0.01*	-	-	-	-	-	-	-0.27	0.16	-1.61	0.00	-5.17	0.00
Nucleoside	**2'-Deoxycytidine**	-	-	-	-	-	-	-	-	-	-	-	-	-0.4	0.54	-0.09	0.65	-0.9	0.00
Nucleoside	**5'-Methylthioadenosine**	-0.95	*0.21*	-1.43	*0.00*	-0.76	*0.00*	-1.54	*0.19*	-0.39	*0.58*	-0.79	*0.83*	-0.56	0.05	-0.73	0.00	-0.89	0.00
Nucleoside	**Adenosine**	-0.95	*0.21*	0.86	*0.01*	1.1	*0.12*	-1.54	*0.19*	-0.39	*0.58*	-0.79	*0.83*	-0.56	0.05	-0.73	0.00	-0.89	0.00
Nucleoside	**Thymidine**	-	-	-	-	-	-	-	-	-	-	-	-	-0.25	0.21	0.17	0.88	-2.14	0.03
Nucleotide	**3'-AMP**	-	-	0.86	*0.01*	1.1	*0.12*	-	-	-	-	-	-	-	-	-	-	0.44	0.94
Nucleotide	**CDP-ethanolamine**	-	-	-	-	-	-	-	-	-	-	-	-	2.51	0.00	-	-	2.85	0.00
Nucleotide	**Cytidine 5'-diphosphocholine**	-	-	-	-	-	-	-	-	-	-	-	-	1.41	0.00	1.67	0.00	1.25	0.01
Nucleotide	**NAD**	4.71	*0.27*	-1.48	*0.00*	-0.55	*0.04*	0.54	*0.24*	-0.03	*0.18*	-0.45	*0.01*	-0.27	0.16	-0.59	0.00	-0.95	0.00
Nucleotide	**NADH**	-0.5	*0.02*	-1.18	*0.00*	-0.48	*0.05*	-	-	-	-	-4.74	*0.00*	-	-	-	-	-	-
Nucleotide	**Uridine**	-0.82	*0.02*	-1.87	*0.00*	-1.03	*0.01*	0.42	*0.36*	-1.05	*0.43*	-1.99	*0.01*	-0.64	0.05	-0.71	0.02	-1.01	0.00
Nucleotide	**Uridine 5'-diphosphogalactose**	-	-	-	-	-	-	-0.05	*0.24*	-0.22	*0.07*	-0.84	*0.01*	-	-	-	-	-	-
Nucleotide	**Uridine 5'-diphosphoglucuronic acid**	-0.6	*0.00*	-1.41	*0.00*	-0.95	*0.00*	0.11	*0.77*	-	-	-	-	-0.54	0.02	-0.9	0.00	-1.94	0.00

Nucleotide	**Uridine diphosphate-N-acetylglucosamine**	-0.49	*0.03*	-1.99	*0.00*	-1.37	*0.00*	-0.86	*0.04*	-0.66	*0.03*	-1.69	*0.00*	-0.51	0.03	-1.03	0.00	-2.03	0.00
Nucleotide	**Uridine diphosphategalactose**	-0.91	*0.02*	-1.44	*0.00*	-0.58	*0.01*	-	-	-	-	-	-	-0.72	0.02	-1.13	0.00	-2.66	0.00
PC	**1,2-Dipalmitoleoyl-sn-glycero-3-phosphocholine**	-	-	-3.11	*0.01*	-2.79	*0.03*	0.47	*0.25*	-1.75	*0.13*	-1.31	*0.06*	-	-	-	-	-	-
PC	**LysoPC(14:1(9Z)/0:0)**	-1.74	*0.58*	-3.65	*0.00*	-2.42	*0.01*	-	-	-	-	-	-	-	-	-	-	-	-
PC	**LysoPC(24:1(15Z))**	-2.41	*0.53*	-2.05	*0.04*	-1.76	*0.17*	0.75	*0.30*	-1.42	*0.22*	-2.09	*0.05*	-2.55	0.03	-4.21	0.00	-3.98	0.01
PC	**LysoPC(P-16:0/0:0)**	-1.87	*0.31*	-0.97	*0.11*	-1.33	*0.20*	-	-	-	-	-	-	-1.88	0.05	-3.34	0.01	-3.25	0.01
PC	**PC(16:0/18:1(9Z))**	-	-	-0.82	*0.22*	-0.68	*0.76*	0.42	*0.27*	-1.48	*0.26*	-1.24	*0.05*	-0.62	0.13	-2.79	0.00	-2.88	0.00
PC	**PC(16:0/18:3 (9Z,12Z,15Z))**	-4.22	*0.31*	-0.46	*0.11*	-1.24	*0.12*	0.45	*0.24*	-	-	-	-	-0.48	0.33	-1.25	0.01	-1.52	0.03
PC	**PC(18:1(9Z)e/2:0)**	-	-	-0.49	*0.14*	-1.53	*0.14*	0.52	*0.49*	-1.36	*0.14*	-1.86	*0.01*	-2.8	0.03	-3.98	0.00	-3.3	0.01
PE	**1-oleoyl-2-linoleyl-sn-glycero-3-phosphoethanolamine**	-0.81	*0.07*	-2.51	*0.00*	-1.81	*0.00*	-	-	-	-	-	-	-0.58	0.27	-1.57	0.02	-3.21	0.00
PE	**1-Palmitoyl-2-linoleoyl PE**	-0.81	*0.07*	-2.65	*0.00*	-1.61	*0.01*	0.02	*0.85*	-0.88	*0.26*	-0.29	*0.46*	-	-	-	-	-	-
PE	**LysoPE(18:0/0:0)**	-	-	-1.93	*0.34*	-1.02	*0.37*	-	-	-	-	-1.17	*0.15*	-2.13	0.03	-2.82	0.00	-1.44	0.06
PE	**LysoPE(18:1(9Z)/0:0)**	-1.23	*0.01*	-2.06	*0.00*	-1.09	*0.00*	0.79	*0.12*	-	-	-	-	-	-	-	-	-	-
PE	**PE(16:0/22:6 (4Z,7Z,10Z,13Z,16Z,19Z))**	-0.05	*0.72*	-0.68	*0.01*	-0.12	*0.28*	-	-	-1.27	*0.55*	-	-	-	-	-	-	-	-
PE	**PE(18:0/20:4 (5Z,8Z,11Z,14Z))**	-	-	-0.1	*0.14*	0.15	*0.13*	1.43	*0.32*	-0.51	*0.40*	0.17	*0.62*	2.08	0.40	1.74	0.72	1.64	0.41
PE	**PE(P-16:0/20:4 (5Z,8Z,11Z,14Z))**	0.51	*0.72*	0.04	*0.47*	0.6	*0.48*	-	-	-0.34	*0.15*	-	-	-	-	-	-	-	-
Peptide	**Carnosine**	5.16	*0.00*	-0.22	*0.42*	0.04	*0.78*	-0.15	*0.27*	-0.44	*0.01*	-0.36	*0.03*	-0.93	0.04	-1.16	0.00	-1.53	0.00
Peptide	**L-Glutathione (reduced)**	-1.02	*0.00*	-3.26	*0.00*	-1.35	*0.00*	-0.04	*0.37*	-0.29	*0.10*	-1.65	*0.01*	-0.63	0.01	-1.24	0.00	-1.72	0.00
Peptide	**L-Glutathione (oxidized)**	-	-	1.48	*0.01*	-	-	1.24	*0.12*	-	-	-	-	-0.17	0.56	-	-	-	-
Peptide	**Ophthalmic acid**	5.85	*0.08*	-2.18	*0.00*	0.2	*0.36*	0.38	*0.00*	0.52	*0.00*	0.82	*0.01*	1.59	0.00	1.62	0.00	1.47	0.00

Peptide	**Pro-leu**	8.41	*0.00*	-1.03	*0.00*	0.1	*0.97*	0.97	*0.00*	1.22	*0.00*	1.33	*0.00*	-0.22	0.73	-0.11	0.69	-0.45	0.00
Phenylketone	**Kynurenine**	-1.65	*0.27*	-	-	-	-	-	-	-0.28	*0.44*	1.24	*0.08*	-	-	-	-	-	-
Polyamine	**N-Acetylputrescine**	-1.25	*0.00*	-2.83	*0.00*	-2.4	*0.00*	-	-	-	-	-	-	-	-	-	-	-	-
Polyamine	**N1,N12-Diacetyl spermine**	1.84	*0.40*	3.11	*0.00*	5.71	*0.00*	3	*0.00*	3.68	*0.00*	4.5	*0.00*	4.79	0.00	4.4	0.00	5.44	0.00
Polyamine	**N1,N8-Diacetyl spermidine**	1.03	*0.00*	0.5	*0.00*	2.15	*0.00*	1.13	*0.00*	1.37	*0.00*	0.71	*0.01*	1.27	0.00	0.53	0.00	0.5	0.01
Polyamine	**N8-Acetyl spermidine**	8.44	*0.02*	0.73	*0.00*	2.71	*0.00*	1.01	*0.32*	1.22	*0.00*	0.77	*0.00*	1.03	0.00	0.62	0.00	0.04	0.80
PUFA	**Alpha-Linolenic acid**	-	-	0.61	*0.93*	1.98	*0.37*	-0.29	*0.60*	-1.03	*0.83*	0.31	*0.62*	-1.26	0.52	-1.34	0.59	-1.47	0.52
PUFA	**Linolenelaidic acid**	-	-	2.32	*0.96*	-1.85	*0.02*	0.05	*0.53*	-1.74	*0.17*	1.01	*0.26*	-1.36	0.59	-2.73	0.18	0.01	0.52
Pyridine	**Pyridoxal**	-	-	0.82	*0.10*	0.24	*0.93*	1.31	*0.53*	1.01	*0.71*	1.04	*0.63*	0.19	0.62	0.22	0.41	0.23	0.76
Pyridine	**Pyridoxamine**	-1.36	*0.17*	-1.96	*0.01*	-0.32	*0.82*	1.79	*0.38*	0.01	*0.80*	0.51	*0.67*	-0.09	0.44	0.06	0.69	-0.48	0.22
Pyridine	**Pyridoxine**	-0.74	*0.01*	-1.5	*0.00*	6.99	*0.00*	-	-	-	-	-1.13	*0.66*	0.6	0.85	1.39	0.04	-	-
Pyrrolidine	**1-Methyl pyrrolidine**	-	-	2.06	*0.02*	0.92	*0.08*	-0.25	*0.23*	0.91	*0.63*	0.16	*0.90*	0.88	0.01	1.01	0.01	1.54	0.00
Pyrrolidine	**Pyrrolidine**	-0.6	*0.34*	-0.89	*0.55*	-0.82	*0.33*	-0.99	*0.65*	-2.59	*0.09*	1.87	*0.50*	-2.09	0.04	-0.07	0.55	-0.25	0.22
SM	**SM(d18:0/14:0)**	-3.11	*0.13*	-2.31	*0.04*	-3.1	*0.10*	-	-	-	-	-	-	-2.34	0.02	-3.86	0.00	-4.08	0.00
SM	**SM(d18:1/16:0)**	-4.02	*0.09*	-5.16	*0.01*	-3.9	*0.04*	1.05	*0.27*	-1.27	*0.29*	-1.2	*0.09*	-2.31	0.04	-3.37	0.00	-4.28	0.00

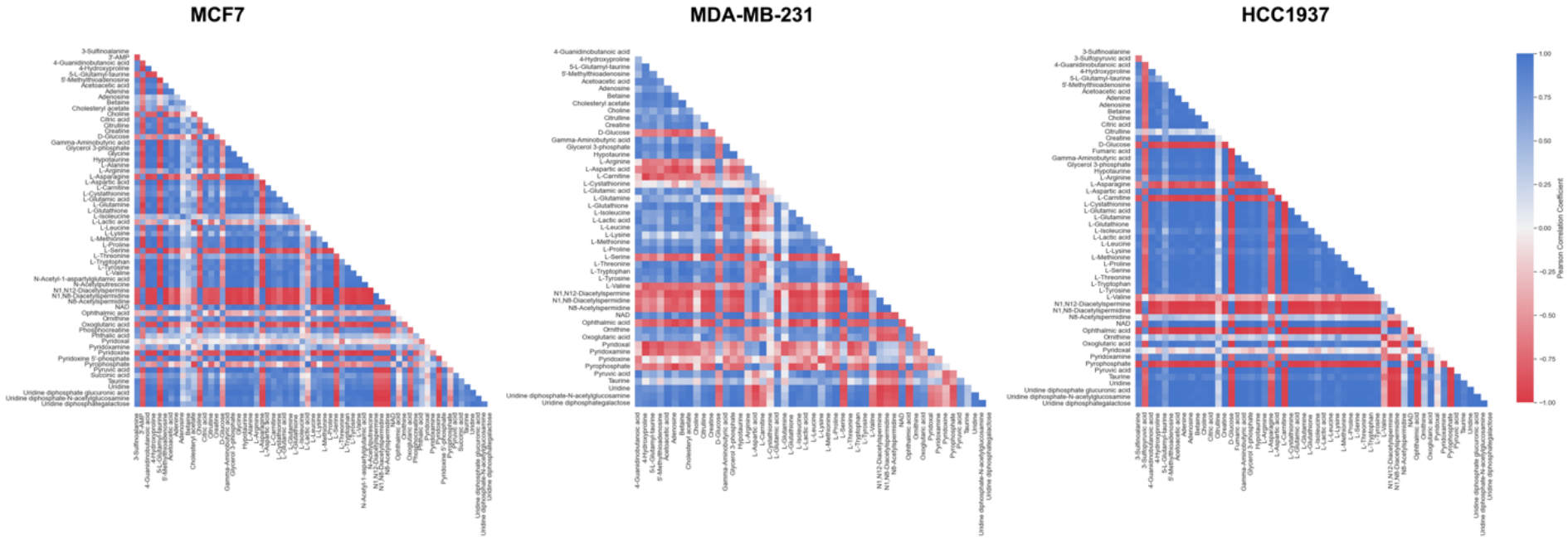

Figure S 4 Pearson's correlation analysis between the relevant metabolites identified within each different breast cancer cell line. Pearson's coefficient is set in a range of 1 to -1, indicative of a positive and negative correlation, respectively.

Table S 5 Chemical properties of the identified amino acids altered upon treatement with IC_{50} dose of Olaparib.

Name	Polarity	S	N	O	C:H
Glutamine	Polar	-	2	3	0.5
Arginine	Polar	-	4	2	0.4
Proline	Non-polar	-	1	2	0.6
Methionine	Non-polar	1	1	2	0.5
Glycine	Non-polar	-	1	2	0.4
Threonine	Polar	-	1	3	0.4
Taurine	Zwitterion	1	1	3	0.3
Hypotaurine	Zwitterion	1	1	2	0.3

Alanine	Non-polar	-	1	2	0.4
Asparagine	Polar	-	2	3	0.5
Aspartate	Polar	-	1	4	0.6
Serine	Polar	-	1	3	0.4